Chemical Engineering Journal 523 (2025) 168222

Contents lists available at ScienceDirect

Chemical Engineering Journal

journal homepage: www.elsevier.com/locate/cej

Experimental study on the gasification characteristics of biomass pyrolysis semi-coke driven by concentrated solar energy

Jinhong Yu, Shiquan Shan *, Shizhun Liu, Zhijun Zhou, Zhihua Wang, Kefa Cen

State Key Laboratory of Clean Energy Utilization, Zhejiang University, Hangzhou, 310027, Zhejiang, PR China

ARTICLE INFO

Keywords:
Concentrated solar energy
Gasification
Biomass
Pyrolysis semi-coke
Energy upgrade factor
Kinetic analysis

ABSTRACT

Solar-driven biomass gasification technology integrates two renewable energy sources in a complementary manner, enabling efficient solar energy storage and the clean, high-efficiency utilization of biomass. As an emerging approach, it holds significant potential. In this study, the gasification of biomass pyrolysis semi-coke (PC) driven by concentrated solar energy is investigated. The CO_2 gasification performance of biomass PC was systematically studied using a self-developed solar-driven gasification–thermogravimetric experimental platform. Key influencing factors, including pyrolysis temperature, biomass type, reactant gas flow rate, catalyst type, and radiative power, were comprehensively examined. The results indicated that the maximum total absorptance of bamboo PC reached 0.91, which was 0.58 higher than that of the raw bamboo. Furthermore, low-ash biomass exhibited superior gas yields and energy conversion efficiency. K_2CO_3 and Na_2CO_3 catalyst were proved to be effective, increasing the peak CO production rate by 54.5 % and 11.8 %, respectively. Kinetic analysis revealed that the activation energy for the solar-driven gasification for bamboo PC was 96.00 kJ/mol, with a pre-exponential factor of 9.399 s^{-1}. Under a solar simulator with a power of 5.2 kW, the total yields of CO and H_2 reached 143.8 mmol/g and 10.1 mmol/g, respectively. Correspondingly, the maximum energy upgrading factor reached 1.41, and the H_2/CO ratio rose to 7.05 %. Collectively, these findings provide robust experimental support for optimizing solar-driven biomass PC gasification technology and accelerating its application in the field of renewable energy.

1. Introduction

To address the global climate issue [1], countries around the world are actively exploring and developing renewable energy. Solar energy, as a renewable and clean resource, holds great promise for solving the energy and environment problems [2]. However, its intermittent and instability remain a significant limitation [3]. Recently, due to growing demand for sustainable energy [4], solar-driven energy conversion technologies have attracted increasing attention [5]. On the other hand, biomass, accounting for approximately 10 % of global energy consumption [6], is a vital carbon-neutral energy source with a potential availability exceeding 100 EJ/year [7]. Gasification technology enables the conversion of biomass into syngas [8]. Nevertheless, conventional gasification methods require the combustion of part of the biomass to supply reaction energy [9], leading to relatively low energy efficiency and failing to meet carbon neutrality goals.

Solar-driven biomass gasification offers significant advantages by synergistically combining two renewable energy [10]. On the one hand, solar radiation provides the necessary thermal energy for the gasification process [11], greatly improving its energy efficiency and reducing carbon emissions. On the other hand, the conversion of solar energy into chemical energy through gasification enables effective energy storage [12]. Compared with conventional gasification, solar-driven biomass gasification exhibits superior energy conversion efficiency, lower CO_2 emissions, and improved syngas quality [13]. Consequently, it has broad application prospects [14] and is increasingly attracting more a research attention [15]. For example, Wu et al. [16] developed a thermochemical energy system based on solar-driven biomass gasification, demonstrating an energy-saving potential of 15.29 % and achieving a maximum energy efficiency of 66.72 %. Similarly, Xu et al. [17] conducted a comprehensive energy analysis of a concentrated solar gasification system, revealing an energy efficiency of 72.86 %. These studies collectively indicate the considerable potential of solar-driven gasification in enhancing energy conversion efficiency [18].

Numerous experimental studies have been conducted on solar-driven gasification, The solar reactor designs are broadly classified into indirect

* Corresponding author.
E-mail address: shiquan1204@zju.edu.cn (S. Shan).

https://doi.org/10.1016/j.cej.2025.168222
Received 7 June 2025; Received in revised form 26 August 2025; Accepted 6 September 2025
Available online 9 September 2025

and direct irradiation configurations [19]. In the field of indirect radiation, Müller et al. [20] designed a 5 kW packed-bed solar reactor for pyrolysis and steam gasification of waste biomass. The experiments successfully produced high-quality syngas with a solar-to-fuel conversion efficiency of 18 %. Similarly, Arriagada et al. [21] developed an indirectly irradiated rotary hybrid porous media solar reactor and investigated the steam gasification of char particles driven by solar energy. Their results indicated that increasing the temperature facilitated a higher H_2/CO ratio. Compared with indirect radiation, direct radiation offers lower thermal resistance in energy transfer and enables higher operating temperatures [22], resulting in superior performance in terms of energy efficiency, gasification characteristics, and economic viability. For instance, Dai et al. [23] developed a solar gasification reactor directly driven by radiation for coal gasification. Under various steam flow rates and feed rates, the peak carbon conversion efficiency reached 70.89 %, with an energy upgrade factor of 1.18. Chuayboon et al. [24] designed a continuously-fed solar reactor to study the effects of temperature and feeding rate on solar-driven biomass steam gasification performance. They reported a carbon conversion close to 97 %, a maximum energy upgrade factor of 1.38, and a solar-to-fuel energy conversion efficiency of 20 %. Wang et al. [25] conducted solar-driven biomass steam gasification experiments and achieved an energy upgrade factor of 1.15 at a radiative power of 3.35 kW, with hydrogen accounting for 47.1 % of the product gas. Zhang et al. [26] developed a solar-driven gasification thermogravimetric (TG) analysis system and demonstrated that the system efficiency of direct radiation gasification was 23.8 % higher than that of indirect radiation, along with enhanced catalytic effects. Using a solar thermogravimetric setup, Zhong et al. [27] explored the reaction mechanism of directly irradiated gasification via the RPM model and determined that the apparent activation energy for willow wood was 117.6 kJ/mol. In addition, Zhao et al. [28] were the first to investigate non-thermal effects in concentrated solar coke gasification, confirming that direct radiation yields greater economic benefits than indirect radiation. In summary, direct radiation offers significant advantages in terms of efficiency and reaction kinetics. However, current experimental studies on direct solar-driven biomass gasification remain limited, and existing mechanistic research often focuses on narrow operating conditions. Therefore, future research should be extended to encompass a wider range of experimental conditions—including different catalysts, reactant gas compositions, and biomass feedstocks—in order to gain a more comprehensive understanding of the energy conversion processes and reaction mechanisms in solar-driven biomass gasification.

In the process of direct solar-driven biomass gasification, several challenges persist. For example, biomass feedstocks typically have low energy density and large volume, which creates difficulties in storage, transportation, and utilization[29]. Moreover, tar produced during pyrolysis can contaminate quartz windows, impairing reactor performance [30]. Converting biomass into pyrolysis semi-coke (PC) before gasification [31] helps mitigate these issues [32]. Therefore, inspired by the integrated approach of coupling pyrolysis and gasification, a carbon-neutral system for solar-driven biomass PC gasification can be constructed, as illustrated in Fig. 1. In this system, the energy required for high-temperature gasification of biomass PC is supplied by concentrated solar radiation, while the heat for pyrolysis and drying is recovered from high-temperature product gases. This effectively utilizes the system's temperature gradient and improves energy efficiency [33]. In addition, the CO_2 gasifying agent used in this system is derived from carbon capture and storage (CCS) technology [26], enabling both CO_2 reduction and its resource utilization. Despite these advantages, systematic experimental investigations on the reaction characteristics of biomass PC gasification under concentrated solar radiation remain limited, highlighting the urgent need for further in-depth research.

Given the above context, this study aims to investigate the energy conversion processes and reaction mechanisms involved in solar-driven biomass PC gasification. To achieve this, a solar-driven biomass PC gasification experimental platform integrated with TG analysis was constructed. A series of experiments were conducted to investigate the influence of several critical parameters on the gasification process, including pyrolysis temperature, biomass type, reactant gas flow rate, catalyst type, and radiative power. The objective is to analyze how these factors influence gasification performance, optimize operating conditions, and enhance both gasification efficiency and the energy quality of the products. Specifically, the research focuses on: (1) Measuring biomass particle radiative properties to identify the optimal stage for solar radiation absorption and assess the benefits of using biomass PC in gasification, providing design insights for solar-driven systems. (2) Conducting gasification experiments to explore the effects of key factors on performance, which will inform biomass and catalyst selection and optimize operating conditions. (3) Using isothermal kinetic analysis based on the Random Pore Model (RPM) model to determine reaction kinetics, including rate constants, activation energy, and pre-exponential factors, thereby verifying non-thermal effects and enhancing understanding of the process. This study provides both experimental data and theoretical insights for optimizing solar-driven biomass gasification technology.

2. Experiments and methods

2.1. Solar-driven gasification experimental platform

In this study, a solar-driven biomass PC gasification-TG experimental

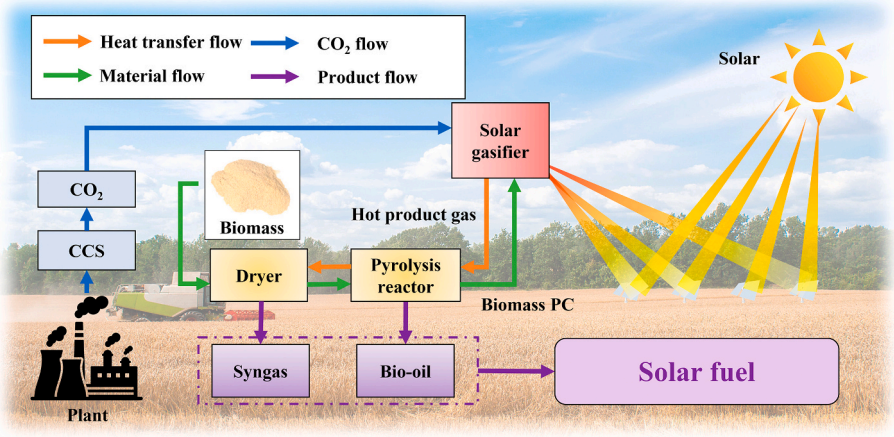

Fig. 1. A carbon-neutral solar-driven biomass PC gasification system

platform was independently constructed, as shown in Fig. 2. The system consisted of a simulated solar light source, a biomass gasification reactor, a thermogravimetric analyzer, and an online flue gas analyzer. The simulated light source was a single xenon lamp with adjustable power (3.2–5.2 kW), used to simulate high-intensity concentrated solar radiation. The spectrum of the light source is shown in Supplementary Material, Fig. S-4. The gasification reactor was based on a T-shaped quartz tube equipped with a convex quartz window and a gas curtain to prevent tar deposition on the window. During experiments, the biomass sample was placed in a circular alumina crucible, which was connected to a high-precision TG analyzer via an alumina rod for real-time mass measurement. A type-K thermocouple (TC1) was positioned at the center of the sample upper surface to monitor its temperature precisely, while three additional type-K thermocouples were placed on both sides of the quartz tube. The reactant gas ($CO_2/N_2 = 1$) entered the reactor from the left side and bottom of the T-shaped tube and exited from the right side. After passing through multiple filters and dryers, the gas was analyzed by an online flue gas analyzer (supplied by MRU, Germany) to determine the composition.

2.2. Materials and radiation characteristic measurement

Agricultural and forestry waste is a major source of biomass, commonly used in biomass gasification and pyrolysis projects [34]. This study selected three representative biomass materials, namely wheat straw, bamboo, and rice hull, as experimental feedstocks. After drying, the raw materials were ground and sieved, with particle samples passing through a 100-mesh screen selected for subsequent experimental analysis. Various biomass PC samples were prepared at different pyrolysis temperature (T_P) using a self-constructed biomass chemical reaction experimental platform. The proximate and ultimate analysis for these materials is provided in Table 1.

The thermal radiation characteristics of biomass particles vary across different stages of the reaction process [35]. These characteristics significantly influence how the particles absorb and utilize solar energy [36]. Therefore, it was crucial to measure the thermal radiation properties of the biomass samples prepared at various pyrolysis temperatures. The sample preparation and reflectance measurement experimental system were illustrated in Fig. 3. Prior to measurement, the samples were compressed into 1 mm thick sheets. The reflectance of bamboo samples at various reaction stages was measured across the 0.3–2.5 μm wavelength range using an ultraviolet-visible spectrometer (AvaSpec-2048XL) and a near-infrared spectrometer (AvaSpec-NIR256–2.5-HSC-EV0), both supplied by Avantes, Netherlands [37]. Assuming that the transmittance of the samples is zero (the validation experiment and analysis of this assumption are provided in Supplementary Material, Fig. S-2), the total solar radiation absorptance of the samples was determined by integrating the spectral hemispherical absorptance over the 0.3–2.5 μm range [38], and was calculated using Eq. (1) as follows:

$$\alpha = \frac{\int_{0.3\mu m}^{2.5\mu m} (1 - R_\lambda) S_{\text{solar,AM1.5}}(\lambda) d\lambda}{\int_{0.3\mu m}^{2.5\mu m} S_{\text{solar,AM1.5}}(\lambda) d\lambda} \tag{1}$$

where, α represents the total absorptance, R_λ is the spectral hemispherical reflectance at wavelength λ, and $S_{\text{solar}}(\lambda)$ is the spectral solar radiative power (AM1.5).

2.3. Performance indicators

Two indicators are used to quantitatively analyze the performance of solar-driven PC gasification, including the carbon conversion ratio and energy upgrade factor. To ensure consistency with related studies and facilitate comparative analysis [23,39], the average carbon conversion ratio is defined as the ratio of the increment of carbon in the product gas to the total carbon content in the raw material [26], and is calculated using Eq. (2) as follows:

$$\overline{X} = \frac{\int \dot{n}_{\text{CO}} dt + \int \dot{n}_{\text{CO}_2} dt + \int \dot{n}_{\text{CH}_4} dt - \int \dot{n}_{\text{CO}_{2,\text{in}}} dt}{n_{\text{PC}}} \tag{2}$$

where $\dot{n}_{\text{CO}}$, $\dot{n}_{\text{CO}_2}$ and $\dot{n}_{\text{CH}_4}$ represent the molar flow rates of CO, CO_2, and CH_4 at the outlet, respectively. $\dot{n}_{\text{CO}_{2,\text{in}}}$ denotes the molar flow rate of CO_2 at the inlet, and n_{PC} refers to the total molar amount of carbon in the biomass PC sample within the crucible.

The energy upgrade factor is an important index for evaluating the performance of solar gasification [15]. This study primarily focuses on the energy processes of solar-driven gasification, with a brief energy analysis of the entire system provided in Supplementary Material, Fig. S-10. It is defined as the ratio of the lower heating value of the product gas to that of the gasification feedstock (in this study, biomass PC prepared from under various pyrolysis temperatures) [39], and is calculated using Eq. (3) as follows:

$$U = \frac{\int \dot{n}_p LHV_p dt}{m_{\text{PC}} LHV_{\text{PC}}} \tag{3}$$

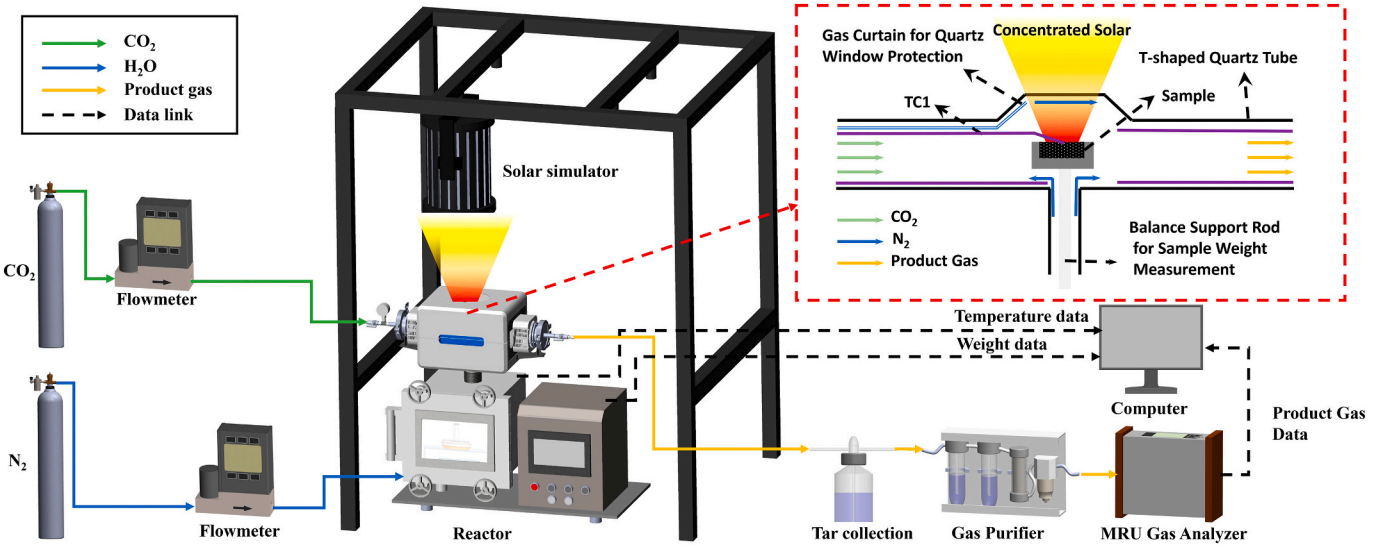

Fig. 2. Schematic diagram of the solar-driven biomass PC gasification-TG experimental platform

Table 1
Proximate analysis and ultimate analysis results of biomass samples[a].

Material	Proximate analysis						Ultimate analysis			
	M%	A_{sh}%	*V%*	*FC%*	$Q_b(j/g)$	*C%*	*H%*	*N%*	*S%*	*O%*
Raw bamboo (T_P = 30 °C)	9.08	0.84	75.41	14.67	17,393	44.36	5.21	0.35	0.58	39.58
Raw rice hull (T_P = 30 °C)	9.27	14.12	61.18	15.43	15,356	38.14	4.43	0.41	0.26	33.37
Raw wheat straw (T_P = 30 °C)	9.93	29.4	48.9	11.73	12,262	30.01	3.53	0.87	0.14	26.12
Bamboo PC (T_P = 600 °C)	5.37	4.14	11.8	78.69	30,631	86.24	2.45	0.51	0.49	0.8
Bamboo PC (T_P = 400 °C)	3.31	3.77	26.3	66.62	27,905	68.62	3.62	0.46	0.27	19.95
Bamboo PC (T_P = 800 °C)	2.68	5.33	4.58	87.41	30,049	89.43	0.8	0.71	0.36	0.69
Rice hull PC (T_P = 600 °C)	3.67	40.44	5.5	50.39	19,049	53.17	1.48	0.44	0.13	0.67
Wheat straw PC (T_P = 600 °C)	2.94	64.3	4.22	28.54	10,756	30.42	1.08	0.78	0.14	0.34

[a] *M*–Moisture, A_{sh}–Ash, *V*–Volatiles, *FC*–Fixed carbon, Q_b–Heating quantity of bomb cylinder, *C*–Carbon, *H*–Hydrogen, *N*–Nitrogen, *O*–Oxygen, *S*—Sulfur.

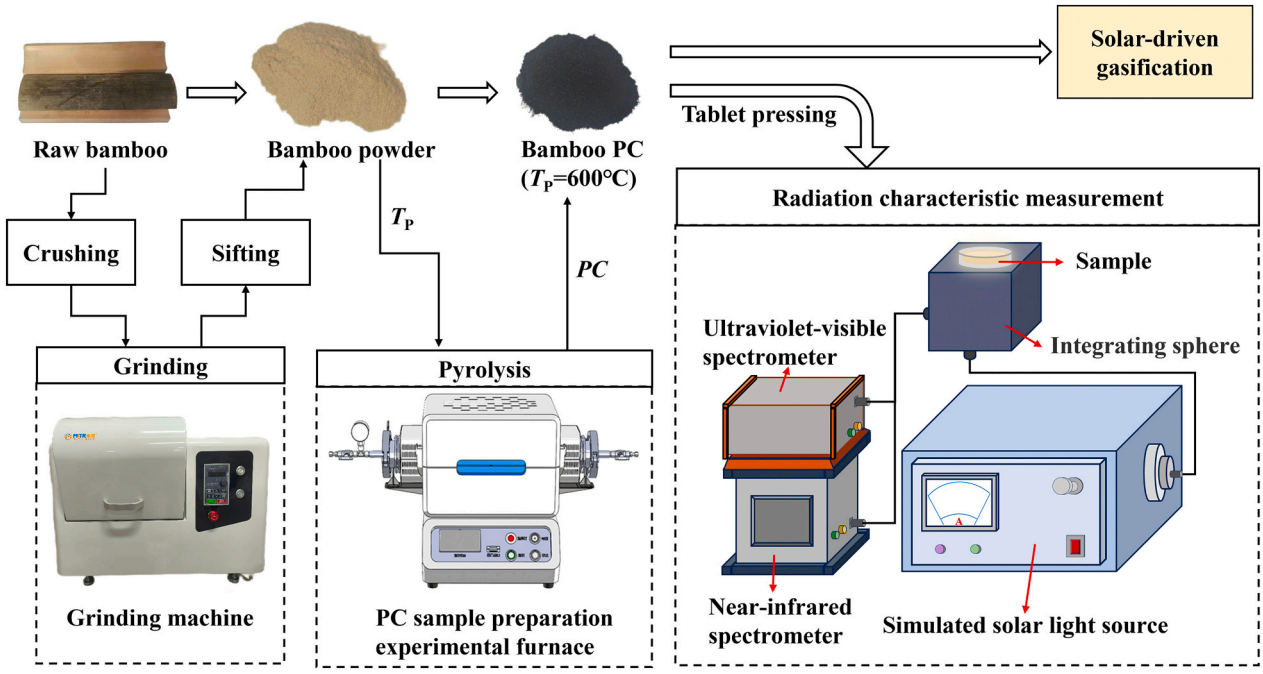

Fig. 3. Schematic diagram of the sample preparation and spectral reflectance measurement experimental system

where $\dot{n}_p$ represents the molar flow rate of the product gas, LHV_P is the lower heating value of the product gas, m_{PC} refers to the total mass of biomass PC placed in the crucible, and LHV_{PC} is the lower heating value of the biomass PC.

2.4. Kinetic models

In this study, a typical isothermal kinetic analysis method was employed to investigate the solar biomass PC gasification process. The Random Pore Model (RPM) accounts for the overlapping effects of pores, the growth of pores during the initial stage of gasification, and the destruction of pores caused by the coalescence of adjacent pores [40]. Therefore, it can predict the maximum reactivity during the reaction process. Compared to the volume and shrinking core models, the RPM is more suitable for biomass PC gasification reactions [41]. In this work, the RPM was used for the kinetic analysis of solar biomass PC gasification, and the reaction rate expression was given as follows:

$$\frac{dX}{dt} = k_{RPM}(1-X)\sqrt{1-\psi ln(1-X)} \tag{4}$$

$$X = \frac{(m_0 - m_t)}{(m_0 - m_\infty)} \tag{5}$$

$$k_{RPM} = A_0 e^{-E/RT} \tag{6}$$

where, *X* represents the sample gasification conversion rate, calculated using Eq. (5). k_{RPM} is the apparent gasification reaction rate constant, which is temperature-dependent and determined using the Arrhenius equation (Eq. (6)). m_0 denotes the initial mass of the sample at the start of gasification, while m_t represents the sample mass at time *t*. m_∞ refers to the mass of ash remaining in the PC after complete reaction. The parameter ψ is used to represent the pore structure of the unreacted sample. Its measurement and determination are provided in Supplementary Material, Tables S-1 and S-2 [42]. A_0、*E* and R are the pre-exponential factor, activation energy, and universal gas constant, respectively.

In the actual calculation, Eq. (4) needs to be linearized, as follows:

$$(2/\psi)\left[(1-\psi ln(1-X))^{1/2} - 1\right] = k_{RPM}t \tag{7}$$

The experimental data obtained from the isothermal thermogravimetric analysis were used to calculate the apparent gasification reaction rate constant k_{RPM}. Subsequently, the activation energy *E* and pre-exponential factor A_0 were determined using the Arrhenius plot ($\ln k_{RPM}$ vs $1/T$), based on Eq. (6).

3. Results and discussion

3.1. Effect of pyrolysis temperature

3.1.1. Biomass PC radiation characteristic

A schematic diagram of the solar radiation absorption process by biomass particles is provided in Supplementary Material Fig. S-1. During solar-driven biomass gasification, solar radiation directly irradiates the particle ensemble, where absorption, reflection, and transmission occur. A higher total absorptance of the particle ensemble indicates a greater proportion of solar radiation being absorbed and utilized, thereby reducing both reflection and transmission losses. Fig. 4 presented the reflectance measurement results of bamboo PC at various pyrolysis temperatures (T_P = 30–800 °C). The results indicated that as T_P increased, the reflectance of the bamboo sample decreases continuously, particularly between 30 °C (raw biomass) and 500 °C (biomass PC), where the decline was most significant. This behavior was attributed to the biomass pyrolysis process primarily occurring between 200 °C and 500 °C [43], coupled with the high volatile content of bamboo PC, which led to the rapid removal of volatiles as T_P increased. This resulted in a shift of the sample's main composition to char, significantly enhancing its absorption properties. As T_P increased from 30 °C to 600 °C, the total absorptance of the bamboo increased sharply from 0.33 to 0.91. However, between T_P = 600 °C and 800 °C, the total absorptance remained nearly constant. Therefore, the removal of volatiles contributed to improving the sample absorption characteristics and helped address the issue of tar contamination during the volatile removal process [30]. Furthermore, biomass PC offered advantages such as high energy density, excellent absorption characteristics, and small particle size [44], which enhanced heat transfer between particles. Thus, PC with T_P of 600 °C was a suitable choice for solar-driven biomass gasification, and was used in subsequent experiments.

3.1.2. Biomass PC gasification performance

In solar-driven biomass PC gasification, the preparation temperature of PC samples and the size of the focal spot significantly affected the gasification process. In the experiments, two focal spot sizes (C1:D = 21 mm, C2:D = 26 mm) and three preparation temperatures (T_P = 400 °C, 600 °C, and 800 °C) were selected to investigate the effects of T_P and focal spot sizes on gasification performance. The experimental conditions were provided in Supplementary Material Table S-3.

Fig. 5 illustrated the CO, H_2, and CH_4 generation rates and total gas yield during the gasification of bamboo PC under different T_P and focal spot sizes. It was evident that as T_P increased, the CO generation rate significantly increased. Specifically, at T_P = 800 °C, the CO generation rate exceeded 3290 μmol/min, which is significantly higher than the rate at T_P = 400 °C, but only slightly greater than at T_P = 600 °C. This indicated that higher T_P enhanced the biomass PC absorption characteristics, thus promoting CO generation. At T_P = 600 °C, the total CO yield reached 123.3 mmol/g, which was much higher than the 93.2 mmol/g at T_P = 400 °C, and slightly higher than the 120.4 mmol/g at T_P = 800 °C. This showed that CO yield first increased and then decreased as the T_P rose. This trend was attributed to the reduction in volatile matter, which increased the proportion of fixed carbon, while the increase in ash content at higher temperatures caused a decrease in the total CO yield at T_P = 800 °C. In contrast, the generation rates of H_2 and CH_4 decreased with increasing T_P, and their total gas yields significantly declined. This was because CH_4 and H_2 mainly originated from the volatile matter and moisture in the PC, and higher T_P led to a substantial reduction in both, thereby inhibiting their generation. Regarding the different focal spot sizes, under the same sample mass, the larger focal spot (D = 26 mm) resulted in faster reaction rates, with higher maximum reaction rates for CO and H_2. The reaction rate was positively correlated with the reaction area. However, the total gas yield at D = 26 mm was lower, as the larger focal spot weakened the radiation intensity at the sample edges, thereby reducing the overall carbon conversion ratio. Overall, selecting an appropriate T_P, and focal spot size can effectively enhanced product gas generation during the gasification process.

Fig. 6 showed the relative weight variation and the calculated k_{RPM} of bamboo PC at different T_P and focal spot sizes. At T_P = 800 °C, the k_{RPM} was 8.53 × 10^{-4} s^{-1}, significantly higher than the 5.44 × 10^{-4} s^{-1} at T_P = 400 °C, and only slightly greater than the 7.76 × 10^{-4} s^{-1} at T_P = 600 °C. This suggested that higher T_P accelerated the gasification reaction. The higher T_P enhanced the thermal radiation absorption properties of bamboo PC, thereby increasing the reaction rate. As discussed, T_P played a crucial role in the gasification process. A higher preparation temperature (T_P = 600 °C) not only increased the reaction rate but also improved the generation rates of CO and H_2, boosted total gas yield, and enhanced energy conversion and carbon utilization efficiency. Additionally, focal spot size impacted the gasification process. A larger focal spot size increased the reaction area, leading to more efficient gasification.

Fig. 7 showed the energy upgrade factor, carbon conversion ratio, and H_2/CO ratio under different T_P and focal spot sizes. As T_P increased,

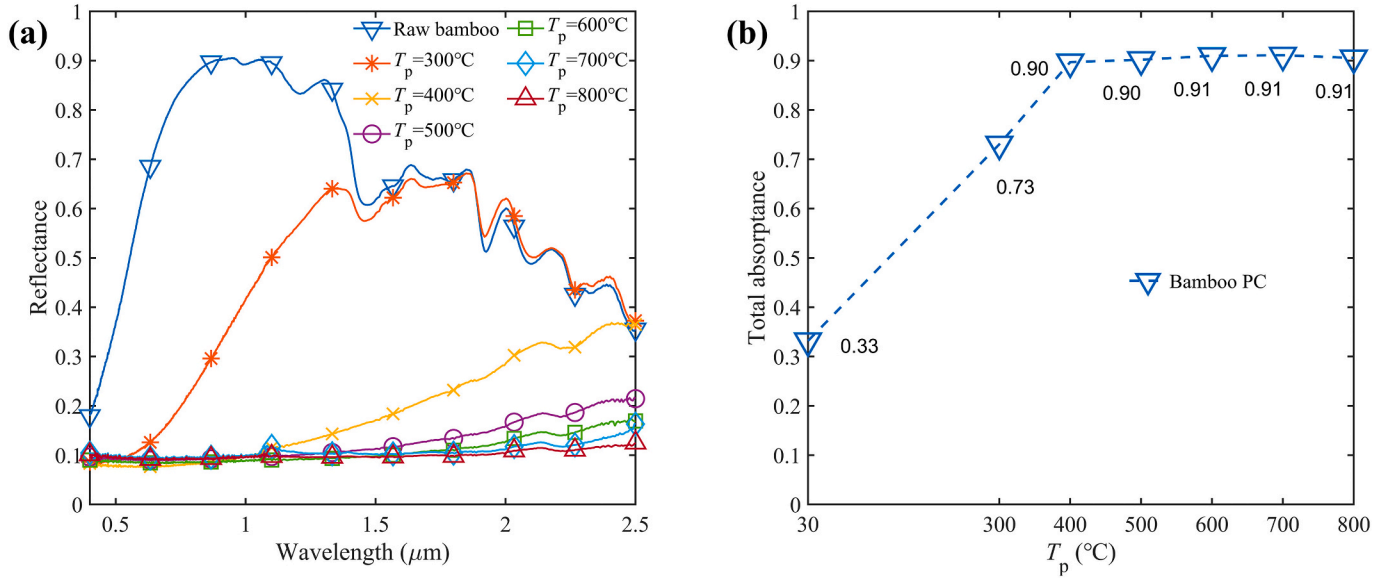

Fig. 4. Radiation characteristics of bamboo PC at different T_P: (a) spectral reflectance, (b) total absorptance.

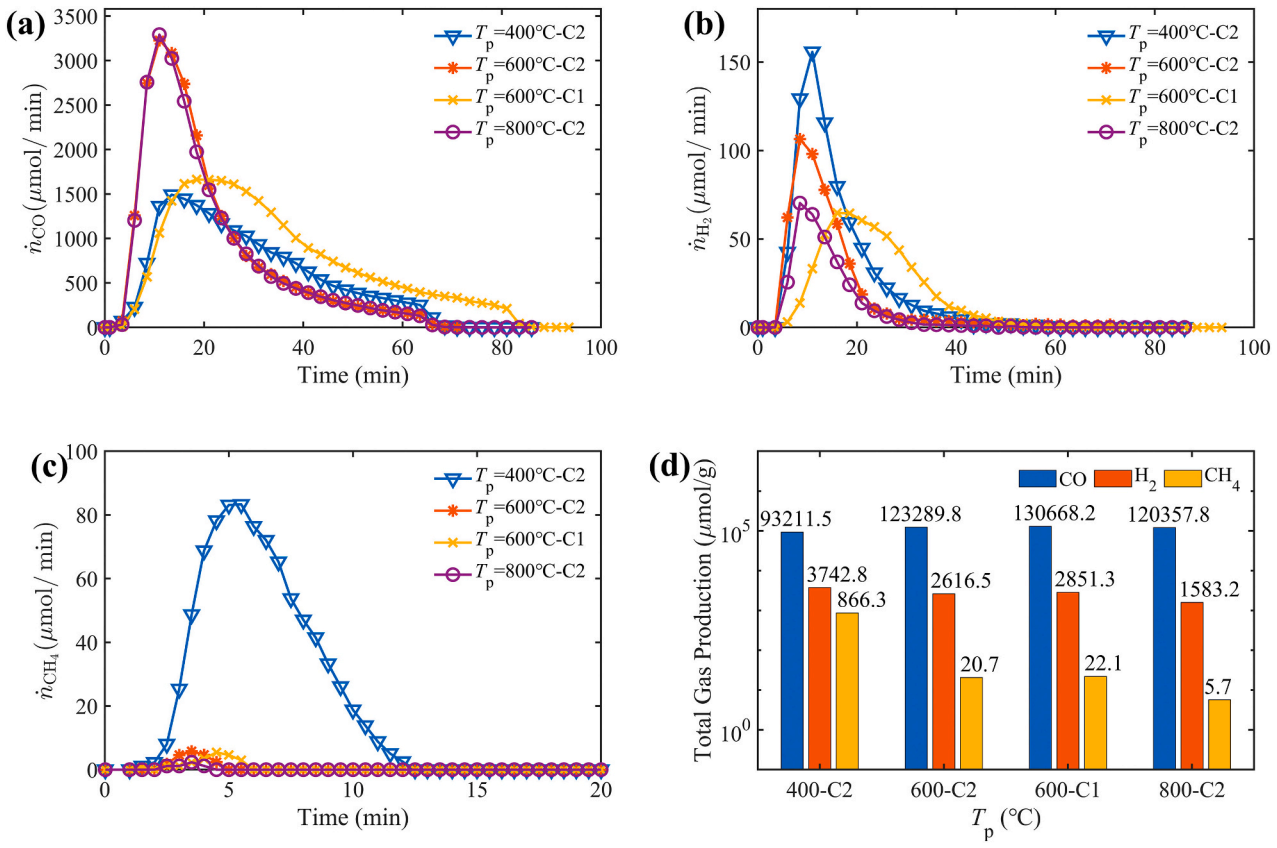

Fig. 5. Effect of T_P on the product gas generation during solar-driven bamboo PC gasification: (a) CO, (b) H_2, (c) CH_4, (d) total gas yield.

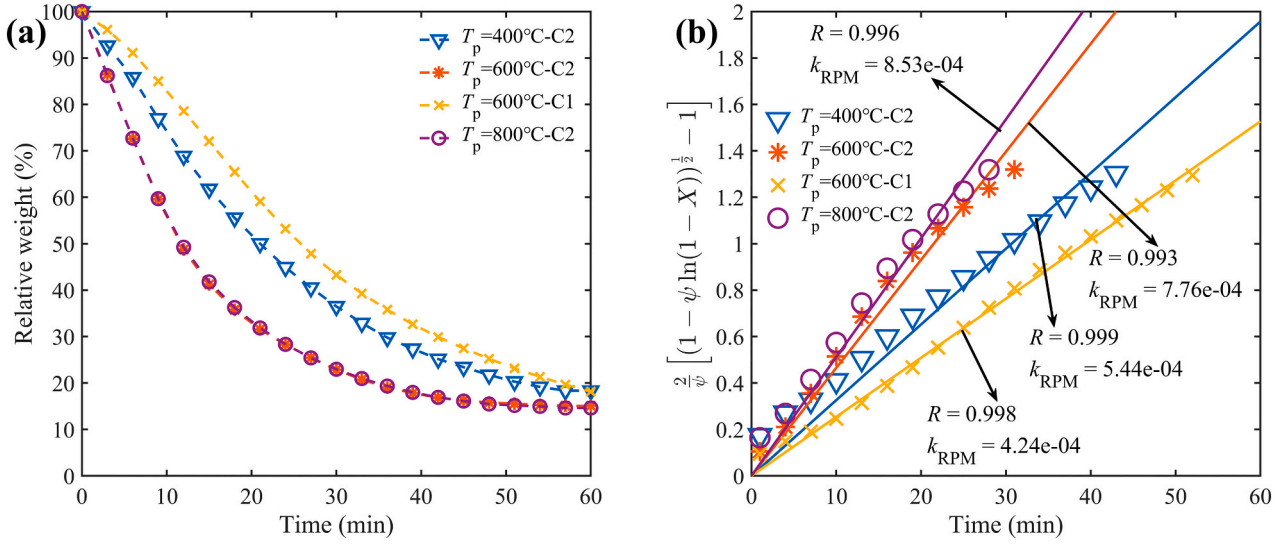

Fig. 6. Apparent gasification reaction rate constants of bamboo PC under different T_P, calculated using the RPM model: (a) relative weight loss over time; (b) fitting results of k_{RPM}.

both the energy upgrade factor and carbon conversion ratio first increased and then decreased. At $T_P = 600$ °C, the energy upgrade factor reached 1.16, and the carbon conversion ratio was 85.8 %, which was higher than the values at $T_P = 400$ °C (1.01 and 83.0 %) and $T_P = 800$ °C (1.15 and 80.8 %). This indicates that a suitable T_P enhanced the gasification performance, improving energy conversion and carbon utilization efficiency. Regarding the focal spot size, the energy upgrade factor and carbon conversion ratio were highest at $D = 21$ mm, with values of 1.23 and 90.9 %, respectively, which were higher than those at $D = 26$ mm. This suggests that a larger focal spot reduces overall gasification performance. The H_2/CO ratio decreased with T_P increasing. Specifically, the ratio dropped from 4.02 % at 400 °C to 1.32 % at 800 °C, primarily due to the reduction of volatile components in the sample. The H_2/CO ratio showed minimal variation under different focal spot sizes, indicating that the focal spot size had little effect on the H_2/CO ratio. Overall, for solar-driven biomass PC gasification, higher T_P and an appropriate reaction area were recommended to significantly enhance the solar gasification performance of biomass PC.

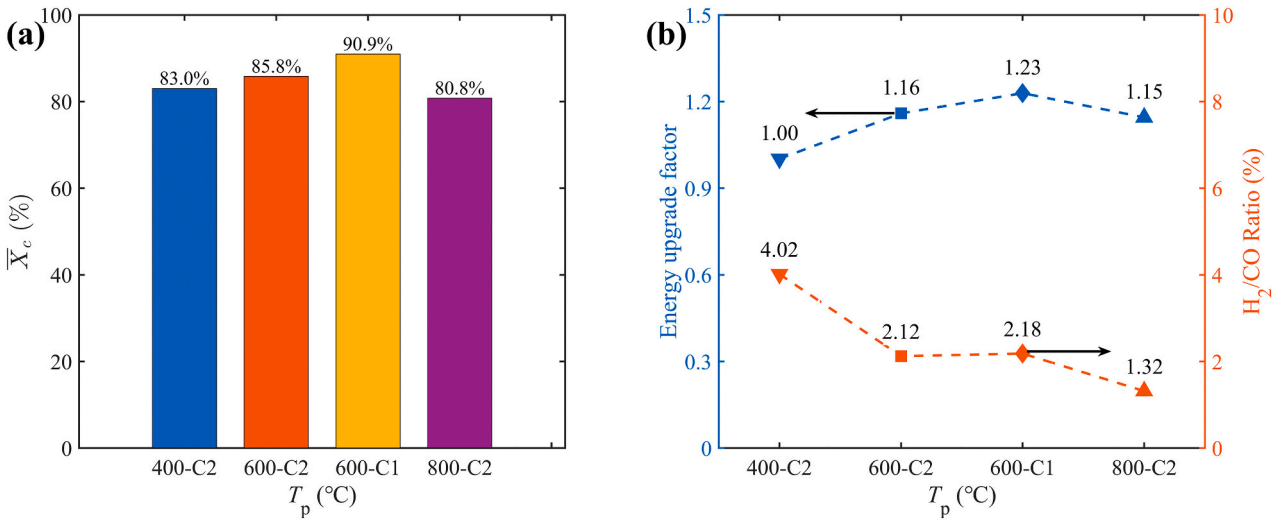

Fig. 7. Effect of T_P on the performance of solar-driven gasification of bamboo PC: (a) carbon conversion ratio, (b) energy upgrade factor, and H_2/CO ratio.

3.2. *Effect of biomass type on gasification performance*

The generation rates of CO and H_2 during the gasification process are closely related to the biomass carbon content, volatile components, and microstructure [25]. Fig. 8 showed the variation in the primary products (CO, H_2, and CH_4) during the gasification of three biomass PCs (bamboo, rice hull and wheat straw), with experimental conditions provided in Supplementary Material Table S-4. As shown, there were significant differences in both the product generation rates and total gas yields among the three biomass PCs. Bamboo PC demonstrated the highest reactivity, with a peak CO generation rate of 1663 μmol/min, substantially exceeding those of rice husk (189 μmol/min) and wheat straw (166 μmol/min). Similarly, bamboo PC also exhibited superior H_2 production. The total gas yield from bamboo was significantly higher than that from rice hull and wheat straw, especially for CO. The total CO yield from bamboo PC was 130.7 mmol/g, while those from rice hull and wheat straw were 19.7 mmol/g and 10.9 mmol/g, respectively, indicating a large disparity. In general, the CO content in the product gas was high for all three biomass PCs, with values of 97.85 %, 98.90 %, and 99.85 %, respectively. In contrast, both the generation rates and total yields of CH_4 were relatively low, confirming that CO and H_2 were the primary products of the gasification process. An analysis of biomass

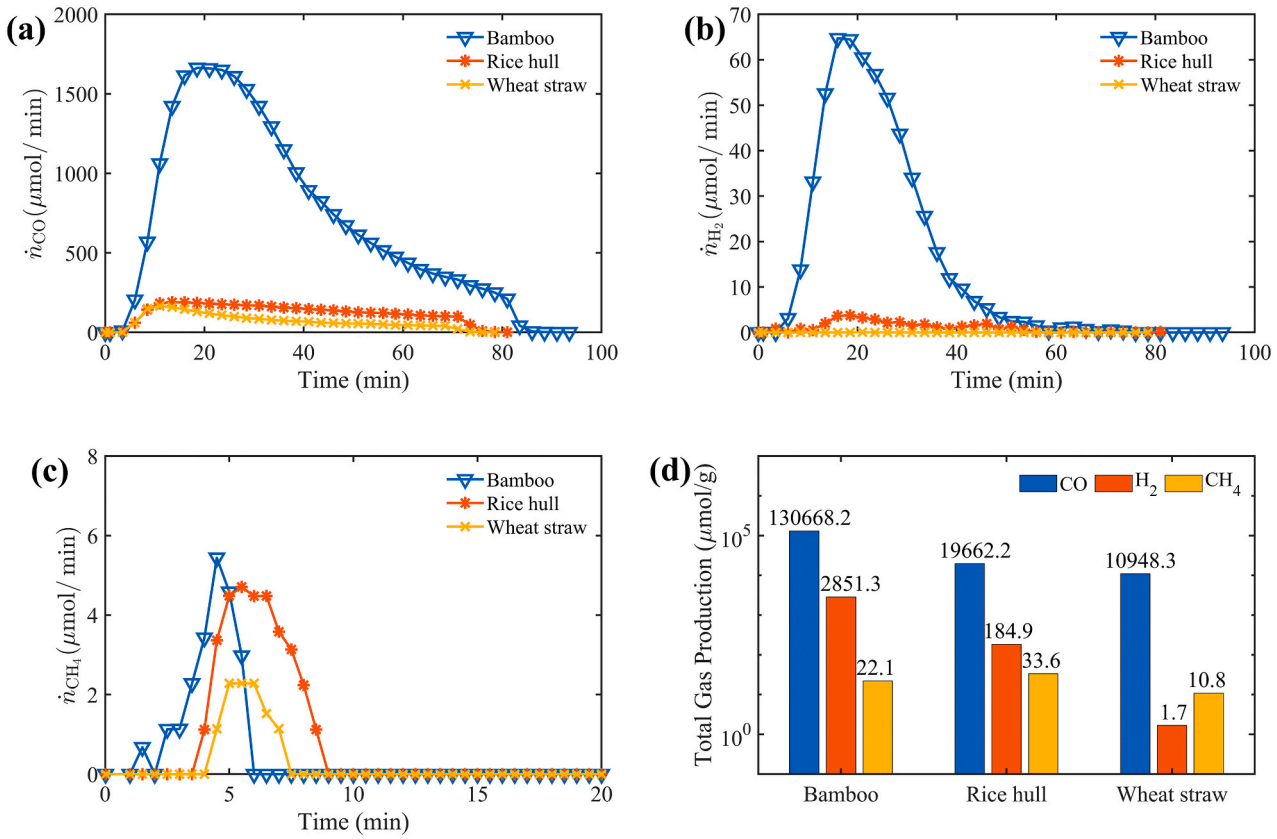

Fig. 8. Effect of biomass types on the product gas generation during solar-driven bamboo PC gasification: (a) CO, (b) H_2, (c) CH_4, (d) total gas yield.

composition revealed that bamboo PC contained 86.24 % carbon and only 4.14 % ash, enhancing its effectiveness in promoting the Boudouard reaction and thereby increasing CO output. Additionally, its higher volatile and moisture contents further contributed to elevated hydrogen production.

Fig. 9 presented the relative weight variation and k_{RPM} for PCs derived from three different biomass types. Fig. 9 (a) showed that the relative weight of bamboo PC decreased rapidly during gasification process, followed by rice hull and wheat straw. The RPM model, due to its consideration of changes in pore structure, effectively fits the gasification experimental data [41]. Fig. 9(b) showed that the k_{RPM} value for bamboo PC was 4.24×10^{-4} s^{-1}, significantly higher than that of rice hull (1.50×10^{-4} s^{-1}) and wheat straw (8.26×10^{-4} s^{-1}), indicating that bamboo underwent a faster gasification reaction. The variation in k_{RPM} values reflected the differences in gasification rates, and the higher value for bamboo PC further confirmed its superior reactivity. Fig. 10 displayed the SEM images of the microstructures of PCs derived from the three biomass types. As shown, bamboo PC, due to its lower ash content, underwent more complete fiber disintegration during volatile matter removal, resulting in finer carbon particles that promoted gasification. In contrast, rice hull and wheat straw samples exhibited large crystalline silica particles, formed by the encapsulation of carbon with a silica layer [45], which significantly hindered the gasification process.

Fig. 11 illustrated the energy upgrade factor, carbon conversion ratio, and H_2/CO ratio of PCs derived from three different types of biomasses. The results showed that the energy upgrade factor of bamboo PC reached 1.23, while those of rice hull and wheat straw PCs were 0.34 and 0.33, respectively. This indicates that bamboo PC was highly effective in converting solar energy and storing it for utilization during solar gasification. In terms of carbon conversion, bamboo achieved a rate of 90.9 %, significantly higher than that of rice husk (25.5 %) and wheat straw (24.8 %). This difference can be attributed to the much higher ash content in rice husk and wheat straw compared with bamboo char, as excessive ash hinders the gasification reaction [46]. According to the compositional analysis of the three types of biomass ash presented in Table 2, the ash of rice husk and wheat straw is predominantly composed of silica, which severely obstructs mass and heat transfer between CO_2 and the biomass char. In contrast, the ash of bamboo contains high proportions of catalytically active elements such as potassium, magnesium, and sodium, which promote the gasification reaction. These findings suggest that bamboo PC not only enabled efficient energy conversion but also facilitated more complete carbon transformation, thereby enhancing both gas yield and overall gasification performance. This further underscored the superiority of bamboo PC as a feedstock for solar-driven gasification. Overall, due to its high carbon content and low ash content, bamboo PC exhibits significantly better gasification performance than rice hull and wheat straw, as reflected in its higher energy upgrade factor and carbon conversion ratio. Therefore, biomass PCs with high carbon and low ash content are more suitable for solar gasification, leading to the production of higher-quality gaseous products.

3.3. Effect of reactant gas flow on gasification performance

In solar-driven gasification of biomass PC, the flow rate of the reaction gas played a critical role in determining the yield of gaseous products [25]. In this study, the input gas mixture had a N_2:CO_2 ratio of 1:1, and the effect of five different reactant gas flow rates (Q_{slpm} = 0.1–0.5 L/min) on gasification performance was investigated. The experimental conditions were detailed in Supplementary Material Table S-5. Fig. 12 illustrated the generation rates and total yields of CO, H_2, and CH_4 during the gasification of bamboo PC under different Q_{slpm}. As the Q_{slpm} increased to 0.4 L/min, the peak generation rates of CO and H_2 increased significantly. At 0.1 L/min, the peak rate of CO was 1075 μmol/min, which increased to 2323 μmol/min at 0.4 L/min, more than double the former, and slightly decreased to 1962 μmol/min at 0.5 L/min. This suggested that higher Q_{slpm} promoted the forward progression of Boudouard reactions, enhancing the gasification reaction rate, while excessively high Q_{slpm} may have inhibited the reaction.

In contrast, the H_2 generation rate decreased sharply at higher Q_{slpm}, particularly at Q_{slpm} = 0.5 L/min, where it dropped to 46 μmol/min, less than half the rate at 0.1 L/min (112 μmol/min). The total yields of CO and CH_4 both increased significantly with increasing Q_{slpm}. At Q_{slpm} = 0.5 L/min, the total CO yield reached 131.4 mmol/g, more than twice the 65.1 mmol/g observed at Q_{slpm} = 0.1 L/min. This indicated that higher Q_{slpm} accelerated the gasification reaction and promoted the formation of CO and CH_4. However, the total yield of H_2 declined as Q_{slpm} increased, with a maximum of 3187.2 μmol/g at 0.1 L/min, dropping to 1882.1 μmol/g at 0.5 L/min. Overall, increasing Q_{slpm} significantly enhanced the generation of CO and CH_4 but inhibited the production of H_2.

Fig. 13 illustrated the relative weight variation and k_{RPM} of bamboo PC under varying Q_{slpm}. As the Q_{slpm} increased, the relative weight of the bamboo PC decreased at an accelerated rate, with the most rapid weight

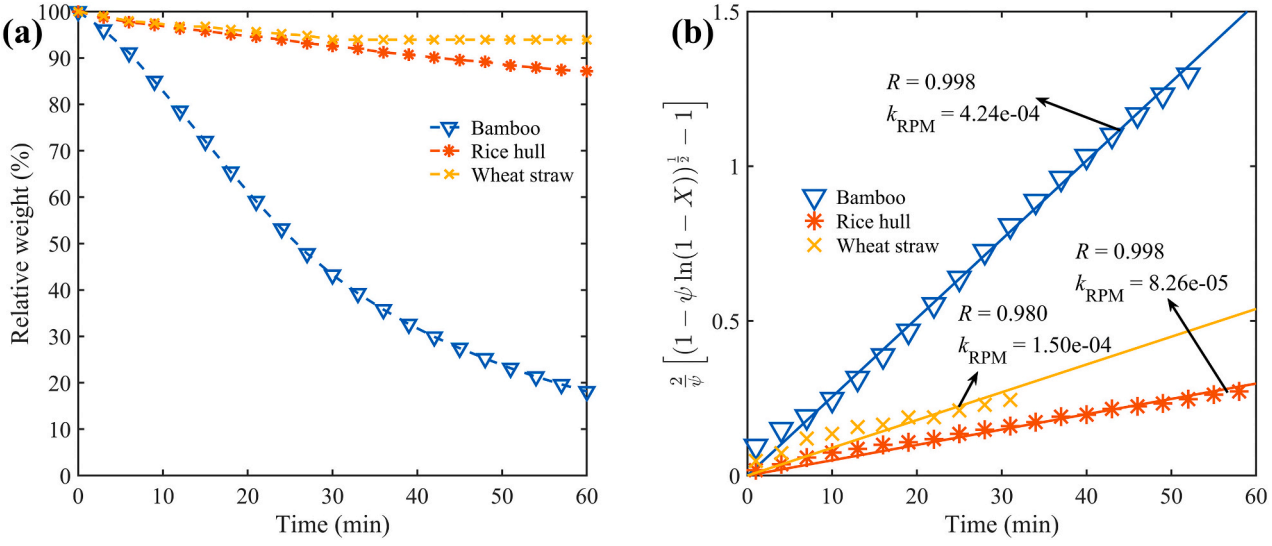

Fig. 9. Apparent gasification reaction rate constants of PCs derived from three different biomass types, calculated using the RPM model: (a) relative weight loss over time; (b) fitting results of k_{RPM}.

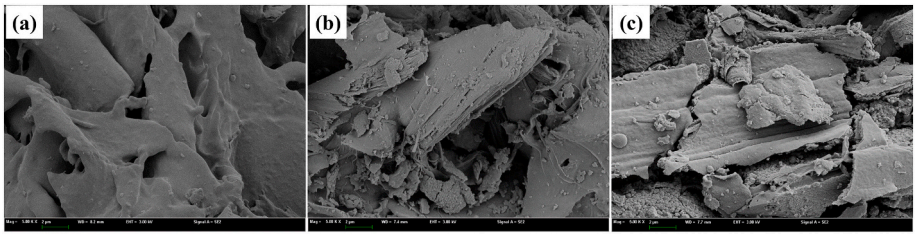

Fig. 10. SEM images comparing the microstructures of PCs derived from different biomass types. (a) Bamboo PC (T_P = 600 °C), (b) Rice hull PC (T_P = 600 °C), (c) Wheat straw PC (T_P = 600 °C).

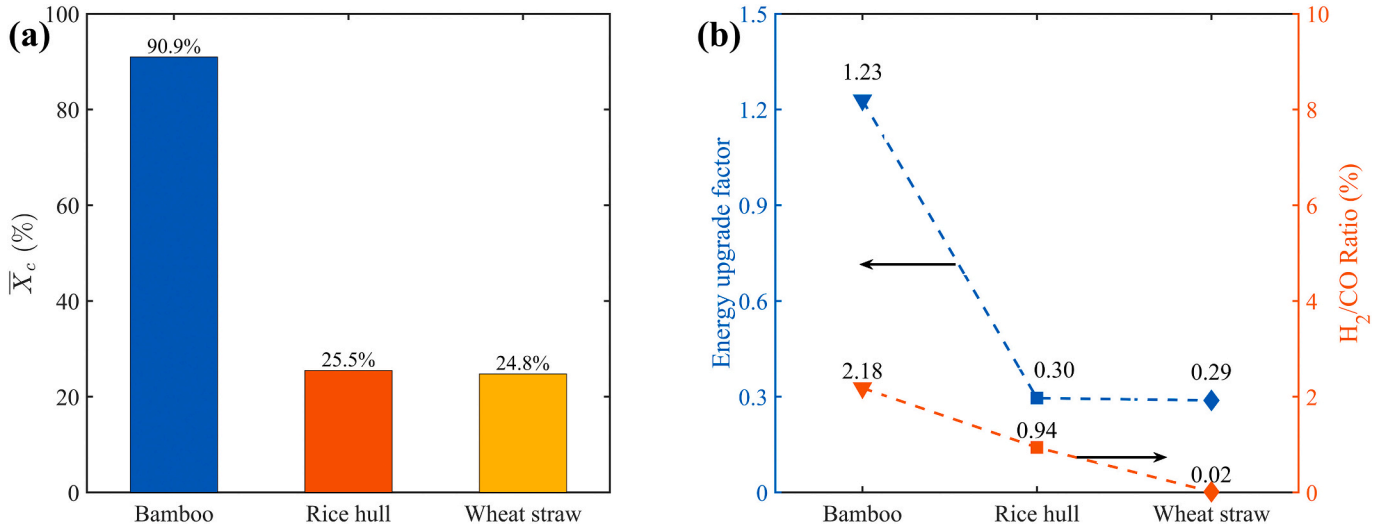

Fig. 11. Effect of biomass types on the performance of solar-driven gasification of bamboo PC: (a) carbon conversion ratio, (b) energy upgrade factor, and H_2/CO ratio.

Table 2
Measured ash composition of three types of biomass

	SiO_2	Al_2O_3	Fe_2O_3	CaO	MgO	K_2O	Na_2O
Bamboo ash	15.08	1.23	0.82	5.74	6.71	35.79	1.05
Wheat straw ash	87.96	1.57	1.76	0.44	2.32	2.19	0.59
Rice hull ash	92.05	0.5	0	0.15	1.27	3.27	1.61

loss observed at Q_{slpm} = 0.4 L/min. As shown in Fig. 13b, the correlation coefficients (R) across different Q_{slpm} conditions ranged from 0.977 to 0.998, indicating that the RPM is well-suited for describing solar-driven gasification of biomass PC. The k_{RPM} value increased with Q_{slpm} initially, reaching a peak of 5.85 × 10^{-4} s^{-1} at 0.4 L/min, which was significantly higher than the 1.97 × 10^{-4} s^{-1} observed at 0.1 L/min. This trend suggested that moderate increases in Q_{slpm} enhanced the gasification reaction, while excessively high flow rates have inhibited it.

Fig. 14 showed the impact of Q_{slpm} on the performance of solar-driven gasification of bamboo PC. As Q_{slpm} increased, both the energy upgrade factor and carbon conversion ratio improved markedly. At 0.1 L/min, the energy upgrade factor was only 0.63, and the carbon conversion ratio was 45.3 %. When Q_{slpm} was increased to 0.2 L/min, the energy upgrade factor increased sharply to 1.22, and the carbon conversion ratio reached 90.1 %. Further increasing Q_{slpm} to 0.5 L/min resulted in only marginal improvements, with values reaching 1.23 and 91.5 %, respectively. These results indicate that a moderate increase in Q_{slpm} enhanced gasification efficiency by promoting higher energy conversion and carbon utilization, while excessively high flow rates offered limited additional benefit.

As shown in Fig. 14b, the H_2/CO ratio decreased with increasing Q_{slpm}. At 0.1 L/min, the ratio was 4.89 %, dropping to 1.43 % at 0.5 L/min. This result suggests that at higher Q_{slpm}, the increased CO_2 concentration in the reaction zone promotes CO formation while suppressing H_2 production, thereby reducing the H_2/CO ratio. The molar concentrations of CO_2 and CO are shown in Supplementary Material Fig. S-9. The higher CO_2 flow enhances its molar concentration, which drives the reverse water gas shift reaction ($CO_2 + H_2 \rightarrow CO + H_2O$). Consequently, H_2 production decreases while CO generation increases, ultimately leading to a lower H_2/CO ratio. Overall, higher Q_{slpm} accelerated the gasification reaction rate, boosted CO and CH_4 production rates, and improved the total gas yield, energy upgrade factor, and carbon conversion ratio. However, high Q_{slpm} also inhibited H_2 production and can led to greater sensible heat losses, which reduced both the reaction rate and the proportion of combustible gases in the output, ultimately hindering the overall efficiency of solar-driven biomass PC gasification.

3.4. Effect of catalysts on the gasification performance

K_2CO_3 [47], Na_2CO_3 [48], and $CaCO_3$ [49] are commonly used catalysts in conventional biomass gasification and have strong catalytic effects on the gasification reaction. However, their performance under solar-driven gasification conditions remains insufficiently explored. In this study, bamboo PC samples (T_P = 600 °C) contained a relatively low ash content (4.14 %), which helped minimize the influence of inherent catalysts on the experimental investigation. Therefore, the bamboo PC was mixed with each of the three catalysts at a 10:1 ratio for experimental evaluation, as detailed in Supplementary Material Table S-6. Fig. 15 showed the generation rates and total yields of the main gaseous products (CO, H_2, and CH_4) during the solar-driven gasification of four blended samples: Bamboo-None, Bamboo-K_2CO_3, Bamboo-Na_2CO_3, and

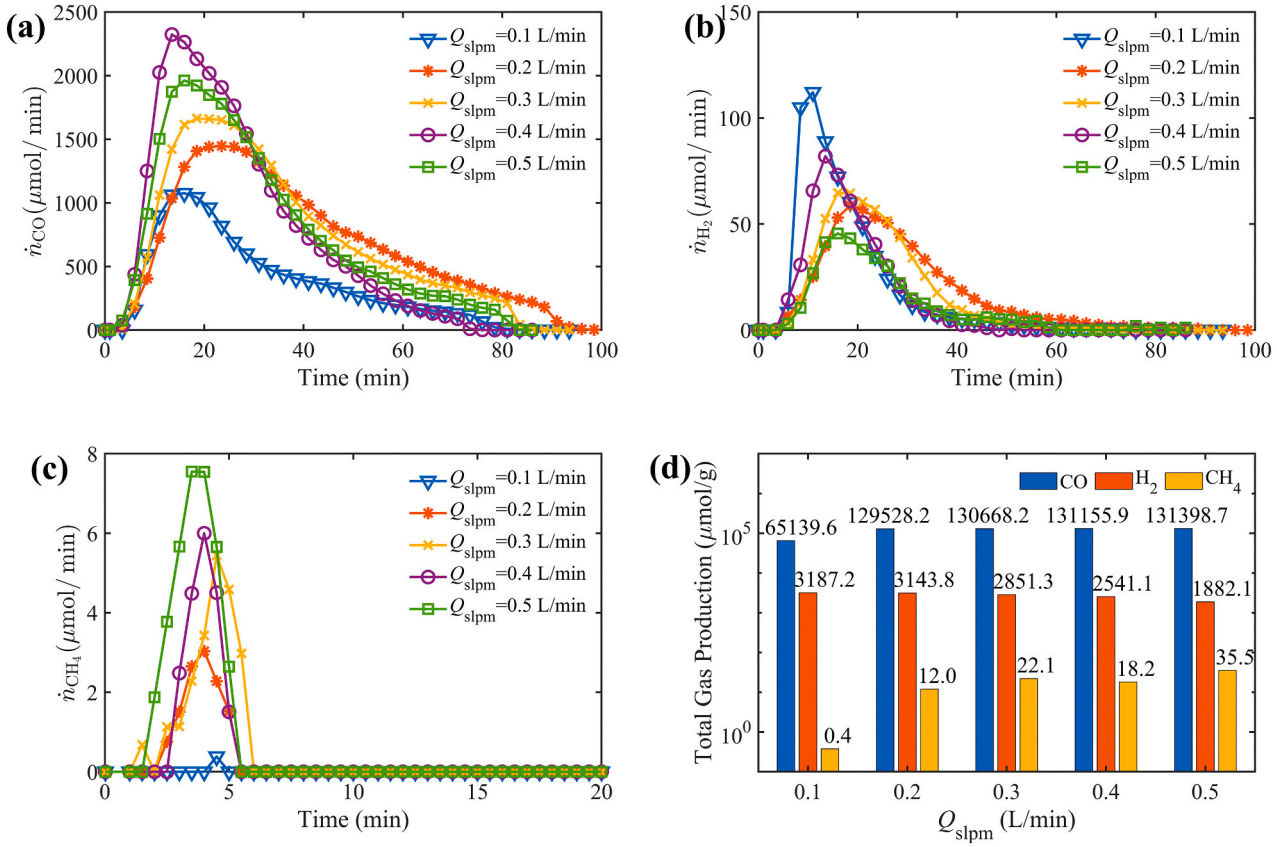

Fig. 12. Effect of reactant gas flow rate on the product gas generation during solar-driven bamboo PC gasification: (a) CO, (b) H_2, (c) CH_4, (d) total gas yield.

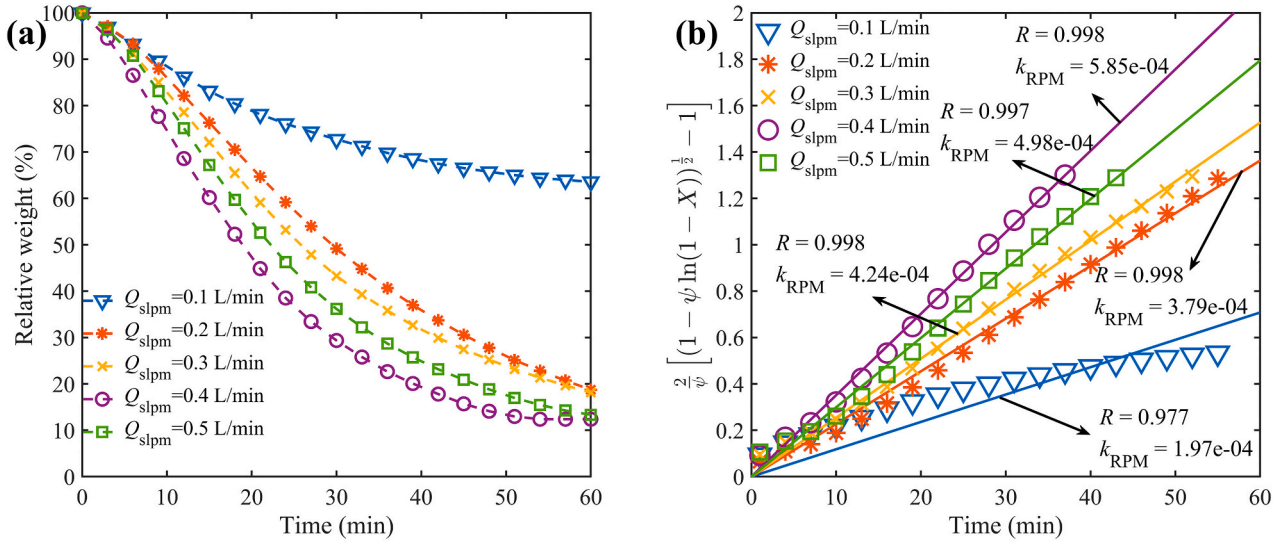

Fig. 13. Apparent gasification reaction rate constants of bamboo PC under different reactant gas flow rate, calculated using the RPM model: (a) relative weight loss over time; (b) fitting results of k_{RPM}

Bamboo-$CaCO_3$. The results showed that catalyst addition significantly influenced the generation rates and total yields of gas products. The peak CO generation rates for Bamboo-K_2CO_3 and Bamboo-Na_2CO_3 reached 2568.8 μmol/min and 1859.4 μmol/min, respectively, which was an increase of 54.5 % and 11.8 % compared to the Bamboo-None sample. This indicated that K_2CO_3 most effectively promoted the Boudouard reaction under solar-driven conditions, thereby enhancing CO production.

Additionally, the samples with K_2CO_3 and Na_2CO_3 showed better H_2 production, particularly during the early stages of gasification. The total gas yield from the Bamboo-K_2CO_3 and Bamboo-Na_2CO_3 were also substantially higher than those of Bamboo-None, with total CO yields of 142.5 mmol/g and 138.0 mmol/g, and total H_2 yields of 3385.8 μmol/g and 3074.4 μmol/g, respectively. In contrast, the Bamboo-$CaCO_3$ sample inhibited the overall gasification process, producing only 127.4 mmol/g of CO and 2195.1 μmol/g of H_2. The CH_4 generation rate is relatively

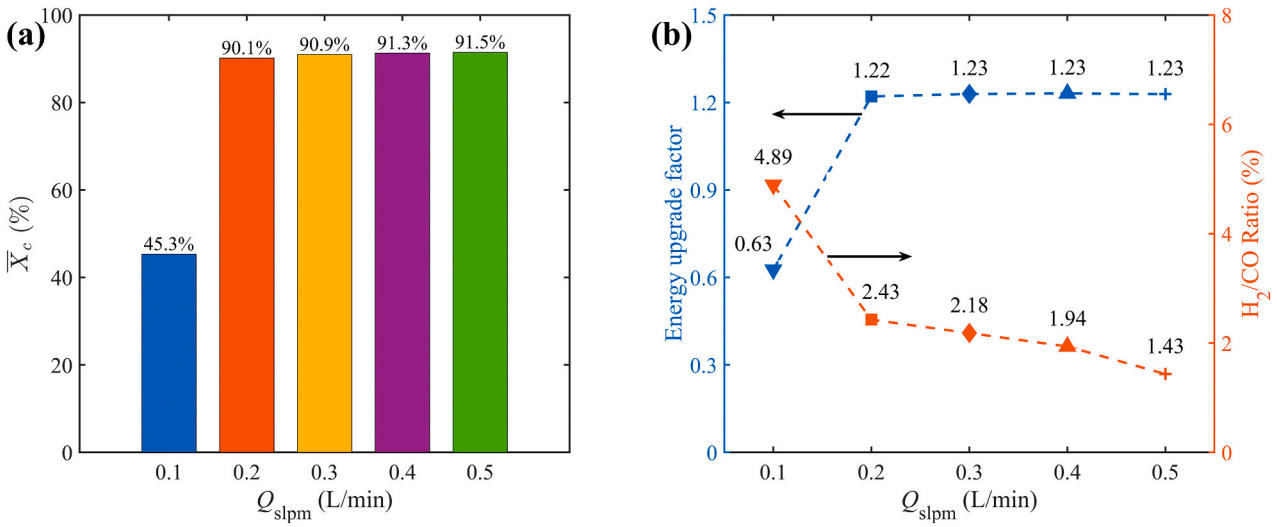

Fig. 14. Effect of reactant gas flow rate on the performance of solar-driven gasification of bamboo PC: (a) carbon conversion ratio, (b) energy upgrade factor, and H_2/CO ratio.

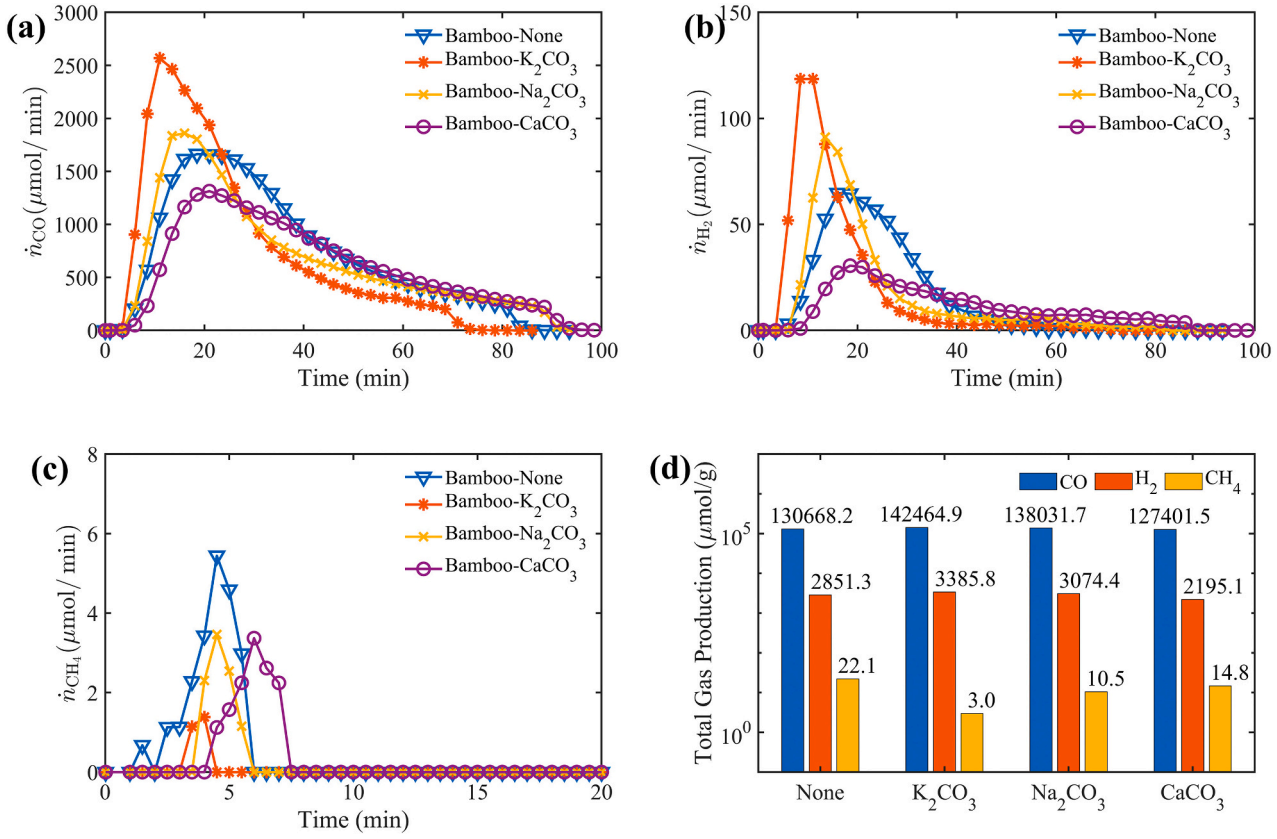

Fig. 15. Effect of different catalysts on the product gas generation during solar-driven bamboo PC gasification: (a) CO, (b) H_2, (c) CH_4, (d) total gas yield.

low and showed little variation among the four samples, indicating that CH_4 was not a primary product during the gasification process. Overall, for solar-driven biomass gasification, K_2CO_3 proved to be the most effective catalyst, significantly lowering the activation energy of the Boudouard reaction, and greatly enhancing the CO and H_2 production. In contrast, $CaCO_3$ exhibited no catalytic effect and even inhibited the solar-driven gasification of bamboo PC.

Fig. 16 presented the relative weight variation and k_{RPM} of four blended samples during the gasification process. The Bamboo-K_2CO_3 exhibited the fastest mass loss, followed by the Bamboo-Na_2CO_3, both exceeding that of Bamboo-None. In contrast, Bamboo-$CaCO_3$ exhibited the slowest mass loss. Fig. 16(b) further showed the k_{RPM} of the four blended samples, calculated using the RPM model. The k_{RPM} value for the Bamboo-K_2CO_3 was 8.27×10^{-4} s^{-1}, significantly higher than those of the other samples, indicating the fastest gasification reaction rate. The k_{RPM} values for the Bamboo-Na_2CO_3 and Bamboo-None samples were 4.90×10^{-4} s^{-1} and 4.24×10^{-4} s^{-1}, respectively, while the Bamboo-$CaCO_3$ sample had the lowest k_{RPM} value of only 3.78×10^{-4} s^{-1}. These results suggested that K_2CO_3 and Na_2CO_3 effectively enhanced the gasification reaction kinetics by lowering the activation energy, thereby

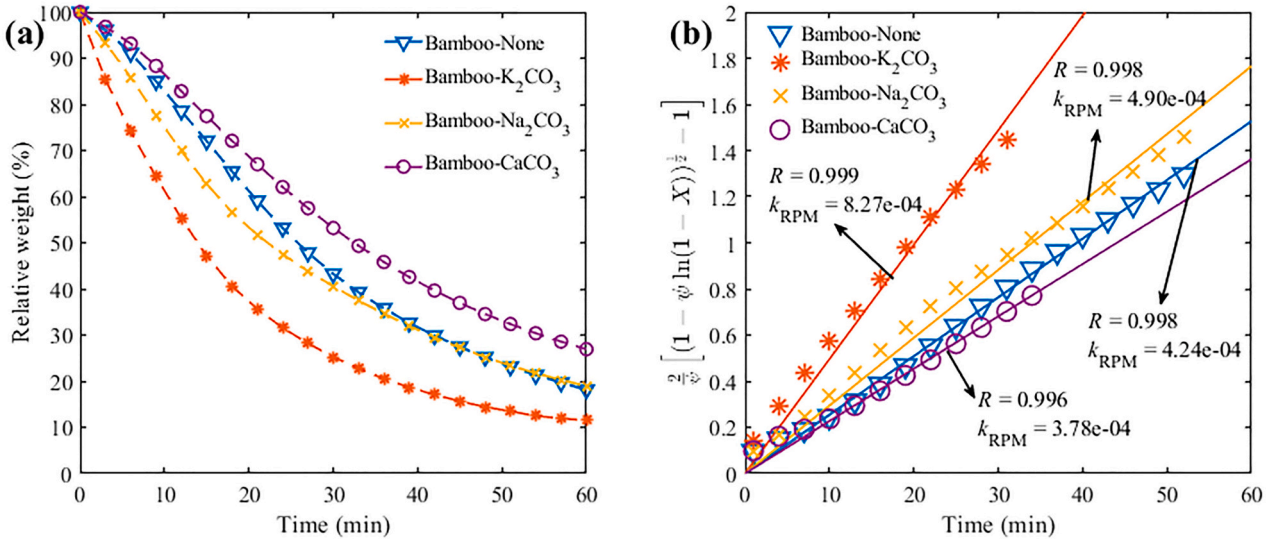

Fig. 16. Apparent gasification reaction rate constants of bamboo PC with different catalysts, calculated using the RPM model: (a) relative weight loss over time; (b) fitting results of k_{RPM}

significantly accelerating the reaction rate, and improving overall gasification performance.

Fig. 17 illustrated the impact of different catalysts on the performance of solar-driven biomass PC gasification. Among the four samples, the Bamboo-K_2CO_3 sample exhibited the highest energy upgrade factor of 1.34 and a carbon conversion ratio of 99.1 %, significantly outperforming the other three samples. The energy upgrade factors for the Bamboo-Na_2CO_3 and Bamboo-$CaCO_3$ samples were 1.34 and 1.19, with corresponding carbon conversion ratios of 96.0 % and 88.7 %, respectively. These results indicated that K_2CO_3 not only significantly enhanced the gasification reaction rate but also effectively promoted solar energy conversion and efficient carbon utilization. Na_2CO_3 also demonstrated good catalytic effects, improving gas yield to some extent. In contrast, $CaCO_3$ showed inhibitory effects on both the energy upgrade factor and carbon conversion ratio, making it less suitable as a catalyst. Notably, the addition of K_2CO_3 increased the H_2/CO ratio from 2.18 % to 2.38 %, indicating that K_2CO_3 promoted hydrogen production. Overall, K_2CO_3 demonstrated the most superior gasification performance. Additionally, the potassium carbonate catalyst is extremely cost-effective, with a recovery rate exceeding 90 % [13], making it an ideal catalyst for solar-driven biomass PC gasification.

3.5. *Effect of radiative power on gasification performance*

Solar energy is inherently intermittent and variable [50], leading to fluctuations in radiative power during actual operations. Consequently, it was essential to experimentally investigate the impact of radiative power on solar-driven biomass PC gasification. Measurements of radiative power at different electrical power inputs (P_E) were provided in the Supplementary Material (Fig. S-3 and Fig. S-5), with experimental parameters detailed in Table S-7. In this study, when P_E was 3.2 kW, the radiative power was 154.3 W; at P_E = 5.2 kW, it reached a maximum of 314.2 W, with a quartz window transmittance of 95.8 %. Fig. 18 showed the generation rates and total yields of CO, H_2, and CH_4 during the bamboo PC gasification process at various P_E levels (3.2–5.2 kW). As shown, increasing P_E significantly enhanced the generation rates of CO, H_2, and CH_4. Specifically, at P_E = 5.2 kW, the CO generation rate peaked at 3520 μmol/min, with a total CO yield of 143.8 mmol/g, compared to 1663 μmol/min and 130.7 mmol/g at PE = 3.2 kW. This indicates that increasing P_E significantly enhanced the gasification reaction rate and

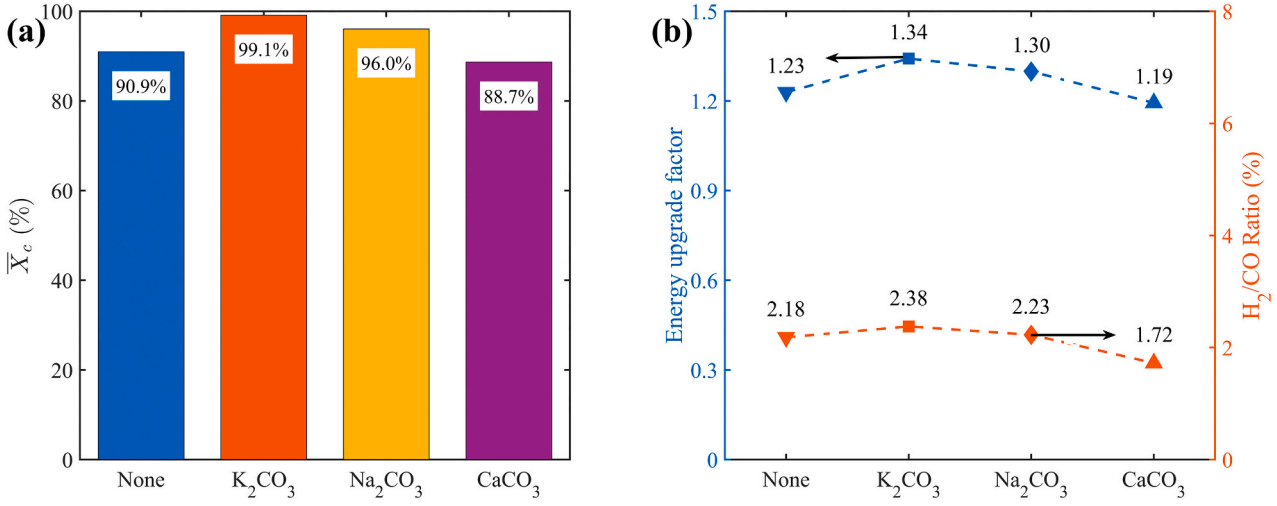

Fig. 17. Effect of different catalysts on the performance of solar-driven gasification of bamboo PC: (a) carbon conversion ratio, (b) energy upgrade factor, and H_2/CO ratio.

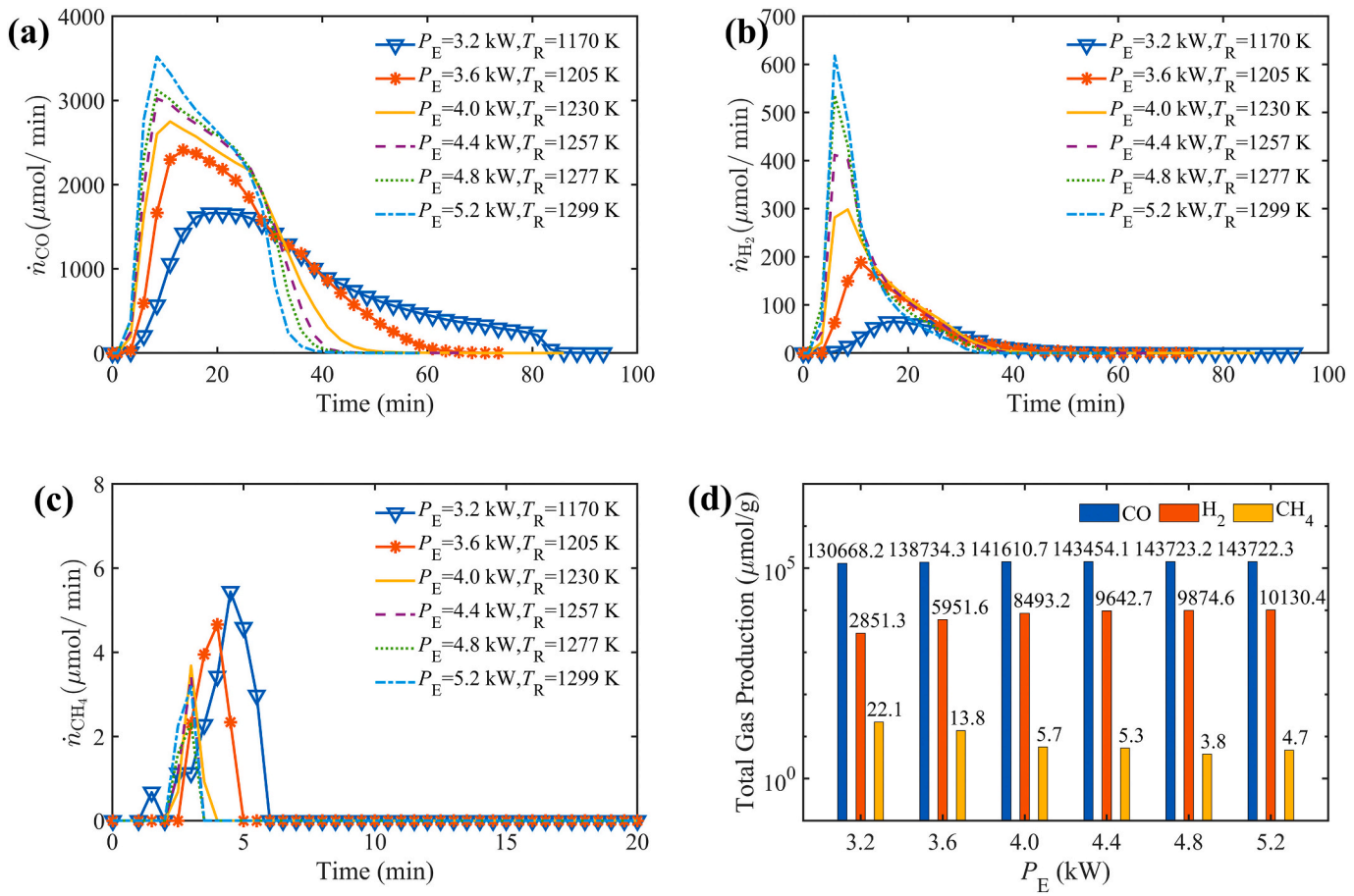

Fig. 18. Effect of P_E on the product gas generation during solar-driven bamboo PC gasification: (a) CO, (b) H_2, (c) CH_4, (d) total gas yield.

gas yield. For H_2, the generation rate gradually increased with rising P_E, reaching 618 μmol/min at $P_E = 5.2$ kW, clearly higher than the 64 μmol/min at P_E = 3.2 kW. In contrast, the CH_4 generation rate remained consistently low with minimal variation, suggesting that CH_4 was not a primary product. Overall, as P_E increased from 3.2 kW to 5.2 kW, the radiative power increase caused the average reaction temperature (T_R) to rise from 1170 K to 1299 K, thereby promoting the gasification reaction. Therefore, increasing radiative power significantly enhanced the generation of CO and H_2 and thus boosting the efficiency of solar-driven biomass PC gasification.

Fig. 19 presented the relative weight variation and k_{RPM} of bamboo PC under different P_E conditions. As shown in the Fig. 19(a), the relative weight loss of the samples increased more rapidly with higher P_E, which was attributed to the rise in reaction temperature, thereby accelerating

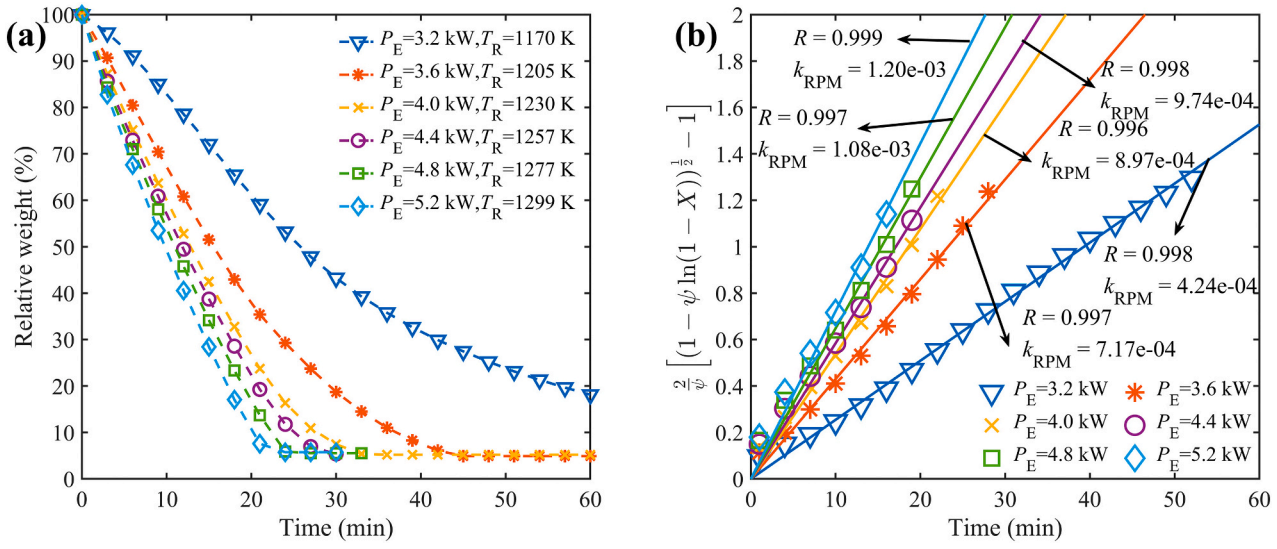

Fig. 19. Apparent gasification reaction rate constants of bamboo PC under different P_E, calculated using the RPM model: (a) relative weight loss over time; (b) fitting results of k_{RPM}.

the reaction rate. During the transition from $P_E = 3.2$ kW to 4.0 kW, the k_{RPM} of the bamboo PC sample increased rapidly from 4.24×10^{-4} s^{-1} to 8.97×10^{-4} s^{-1}. However, when P_E was further raised to 5.2 kW, the rate of increase slowed, with k_{RPM} reaching 1.20×10^{-3} s^{-1}, indicating a diminishing return in reaction rate acceleration. Fig. 20 displayed the Arrhenius plot of k_{RPM} versus $1/T_R$ for bamboo PC under different P_E conditions. A linear fit yielded the activation energy (E) and pre-exponential factor (A_0), with a correlation coefficient (R) of 0.961. The calculated values of E and A_0 were 96.00 kJ/mol and 9.399 s^{-1}, respectively. Furthermore, thermogravimetric experiments of conventional gasification for bamboo char were conducted, and the kinetic parameters were obtained using a non-isothermal analysis method, yielding an activation energy of 332.2 kJ/mol. The detailed experimental results and calculation procedures are provided in the Supplementary Material. Compared with the conventional case, the activation energy for direct radiative gasification decreased by 236.2 kJ/mol, confirming the existence of a non-thermal effect in solar-driven gasification. This finding suggests a relatively low energy barrier for the solar-driven gasification of bamboo char, where increasing radiative power effectively promotes the reaction.

Fig. 21 illustrated the influence of radiative power on the solar-driven gasification performance of bamboo PC. Both the energy upgrade factor and carbon conversion ratio increased substantially as P_E rose. Specifically, when P_E increased from 3.2 kW to 4.4 kW, the energy upgrade factor increased from 1.23 to 1.40, while the carbon conversion ratio improved from 90.9 % to 99.8 %. Beyond 4.4 kW, further increases in P_E yielded only marginal improvements in both indicators. This trend suggested a strong correlation between energy upgrade factor and carbon conversion ratio, and implied that while higher radiative power enhanced energy efficiency and carbon utilization, the energy upgrade factor plateaued as carbon conversion approached 100 %.

Additionally, the H_2/CO ratio increased markedly from 2.18 % to 7.05 % as P_E rose from 3.2 kW to 5.2 kW, indicating that elevated radiative power significantly promoted H_2 production and improved product gas quality. This effect is not solely attributed to thermal phenomena but also involves non-thermal contributions. For example, Zhao et al. [28] reported that under high radiation intensity, graphite carbon exhibits self-catalytic activity that promotes the pyrolysis of biomass carbon, leading to the formation of highly active carbon-chain structures. Such non-thermal effects enhance H_2 generation while suppressing CO production, thereby increasing the H_2/CO ratio, which is consistent with the findings of this study. Overall, the increasing radiative power had a substantial impact on the solar-driven gasification performance of bamboo PC. It enhanced the generation rates and total yields of CO and H_2, raised the energy upgrade factor and carbon conversion ratio, and optimized energy conversion efficiency. The calculated values of k_{RPM}, E and A_0 confirmed that bamboo PC possessed a low energy barrier for solar-driven gasification. Therefore, increasing radiative power significantly accelerated the gasification reaction rate and improved overall system efficiency. These findings offered an experimental foundation for optimizing radiative power configuration and reaction conditions in solar-driven gasification systems.

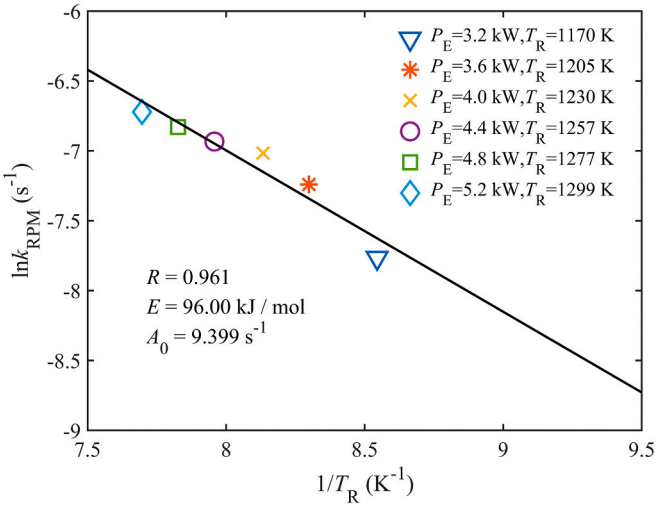

Fig. 20. Arrhenius plots for the RPM models of Bamboo PC.

4. Conclusion

This study measured the radiative characteristics of different biomass PC samples and conducted a series of experimental investigations using a self-constructed solar-driven biomass gasification-TG experimental platform. The study primarily focused on the effects of T_P, biomass type, Q_{slpm}, different catalysts, and radiative power on gasification performance, providing an in-depth analysis of the dynamic reaction process and energy conversion in solar-driven biomass PC gasification. Furthermore, kinetic analysis of bamboo PC was performed based on the RPM model, revealing the E and A_0 factor for the solar-driven gasification of bamboo PC. The main conclusions were as follows:

(1) Volatile removal significantly enhanced the sample absorption characteristics. As the T_P increased to 600 °C, the total absorptance of bamboo PC increased rapidly from 0.33 to 0.91. This suggests that, compared to the original biomass, the biomass PC exhibits a significant advantage in absorbing solar radiation. An optimal T_P improved the energy upgrade factor and energy efficiency of solar-driven biomass PC gasification. At T_P = 600 °C, the energy upgrade factor and carbon conversion ratio were 0.16 and 2.8 % higher, respectively, compared to samples with T_P = 400 °C.

(2) Biomass with high carbon content and low ash content was more suitable for solar-driven biomass PC gasification. The analysis of ash composition reveals that the silica content in the ash significantly inhibits heat and mass transfer during the gasification process, thereby reducing the overall gasification performance. The CO yield of bamboo PC, with an ash content of only 4.14 %, was 111.0 mmol/g and 119.8 mmol/g higher than that of wheat (ash = 64.3 %) and rice husk (ash = 40.44 %) samples, respectively. The energy upgrade factor was 0.93 and 0.94 higher, and the carbon conversion ratio was 65.4 % and 66.1 % higher, respectively.

(3) Increasing the Q_{slpm} enhanced gas generation rate. As Q_{slpm} increased from 0.1 L/min to 0.4 L/min, the peak CO generation rate rose from 1075 μmol/min to 2323 μmol/min. The energy upgrade factor increased by 0.6, and the carbon conversion ratio improved by 46 %. Increasing Q_{slpm} elevated the CO_2 concentration in the reaction zone and reduced the CO concentration, thereby accelerating the Boudouard reaction and optimizing energy conversion and carbon utilization efficiency. However, this also inhibited the water-gas shift reaction, which suppressed H_2 production, while the higher CO_2 concentration in the outlet gas led to increased sensible heat loss and reduced product gas heating value.

(4) Catalysts K_2CO_3 and Na_2CO_3 significantly enhanced solar-driven biomass PC gasification. At a 10 % blended ratio, the peak CO generation rate increased by 54.5 % and 11.8 %, respectively. The energy upgrade factor improved by 0.11 and 0.07, and the carbon conversion ratio increased by 8.2 % and 5.1 %. Due to its excellent catalytic performance, low cost, and ease of recovery, K_2CO_3 shows substantial application potential. In contrast, $CaCO_3$ acted as a gasification inhibitor.

(5) The activation energy for solar-driven bamboo PC gasification was significantly lower than that for conventional gasification, obtained to be 96.00 kJ/mol, and the pre-exponential factor was

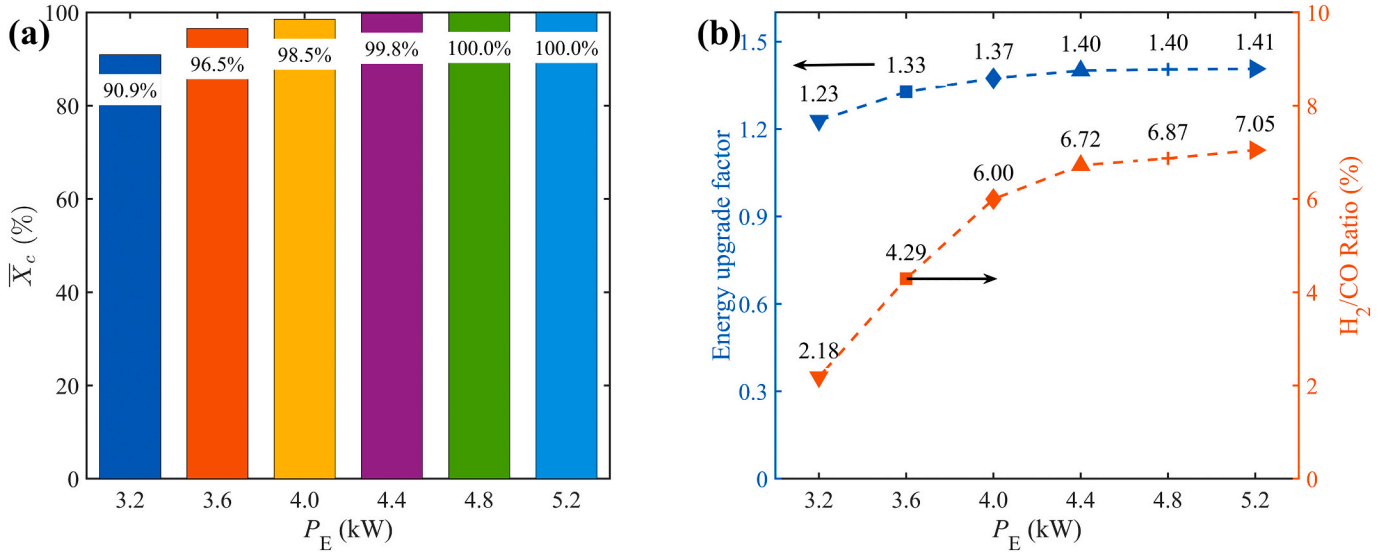

Fig. 21. Effect of P_E on the performance of solar-driven gasification of bamboo PC: (a) carbon conversion ratio, (b) energy upgrade factor, and H_2/CO ratio.

9.399 s^{-1}. This supports the non-thermal effects of directly irradiated gasification. Under $P_E = 5.2$ kW ($T_R = 1299$ K), the peak CO and H_2 generation rates reached 7040 μmol/(min·g) and 1236 μmol/(min·g), respectively. The total yields of CO and H_2 were 143.8 mmol/g and 10.1 mmol/g, with the highest energy upgrade factor of 1.41 and an H_2/CO ratio of 7.05 %. These results confirmed that increasing radiative power significantly enhanced the energy efficiency and product gas generation of solar-driven biomass PC gasification.

CRediT authorship contribution statement

Jinhong Yu: Writing – original draft, Visualization, Validation, Software, Methodology, Investigation, Formal analysis, Data curation. **Shiquan Shan:** Writing – review & editing, Supervision, Resources, Project administration, Methodology, Investigation, Funding acquisition, Conceptualization. **Shizhun Liu:** Writing – review & editing, Software, Investigation. **Zhijun Zhou:** Resources. **Zhihua Wang:** Resources, Project administration. **Kefa Cen:** Resources.

Declaration of competing interest

The authors declare that they have no known competing financial interests or personal relationships that could have appeared to influence the work reported in this paper.

Acknowledgments

This work was supported by Natural Science Foundation of Zhejiang Province (LZ25E060001), National Natural Science Foundation of China (52206175), the Fundamental Research Funds for the Central Universities (2022ZFJH04).

Appendix A. Supplementary data

Supplementary data to this article can be found online at https://doi.org/10.1016/j.cej.2025.168222.

Data availability

Data will be made available on request.

References

[1] IPCC, Global Warming of 1.5°C: An IPCC Special Report, Intergovernmental Panel on Climate Change, Geneva, Switzerland, 2018 https://www.ipcc.ch/sr15/.
[2] Y. Chen, S. Zhang, M. Lin, Operational guidelines for a concentrated solar-driven high-temperature electrolysis reactor beyond thermoneutral voltage, Energ. Conver. Manage. 322 (2024) 119166, https://doi.org/10.1016/j.enconman.2024.119166.
[3] J. Yu, S. Wang, M. Guo, Q. Xu, K. Luo, J. Fan, New concept of solar-driven biomass gasification: an Eulerian-Lagrangian study, Energy 318 (2025) 134876, https://doi.org/10.1016/j.energy.2025.134876.
[4] Y. Xin, X. Xing, X. Li, H. Hong, A biomass–solar hybrid gasification system by solar pyrolysis and PV– solid oxide electrolysis cell for sustainable fuel production, Appl. Energy 356 (2024) 122419, https://doi.org/10.1016/j.apenergy.2023.122419.
[5] G. Wang, Z. Zhang, J. Lin, Multi-energy complementary power systems based on solar energy: a review, Renew. Sustain. Energy Rev. 199 (2024) 114464, https://doi.org/10.1016/j.rser.2024.114464.
[6] K. Abouemara, M. Shahbaz, G. Mckay, T. Al-Ansari, The review of power generation from integrated biomass gasification and solid oxide fuel cells: current status and future directions, Fuel 360 (2024) 130511, https://doi.org/10.1016/j.fuel.2023.130511.
[7] H. Haberl, T. Beringer, S.C. Bhattacharya, K.-H. Erb, M. Hoogwijk, The global technical potential of bio-energy in 2050 considering sustainability constraints, Curr. Opin. Environ. Sustain. 2 (2010) 394–403, https://doi.org/10.1016/j.cosust.2010.10.007.
[8] Y. Ayub, J. Ren, T. Shi, Exploring gasification process and technology for biomass-waste utilization: a comprehensive review on the path to sustainable energy, Process Saf. Environ. Prot. 188 (2024) 1489–1501, https://doi.org/10.1016/j.psep.2024.06.056.
[9] Z. Yao, S. You, T. Ge, C.-H. Wang, Biomass gasification for syngas and biochar co-production: energy application and economic evaluation, Appl. Energy 209 (2018) 43–55, https://doi.org/10.1016/j.apenergy.2017.10.077.
[10] Y. Fang, M.C. Paul, S. Varjani, X. Li, Y.-K. Park, S. You, Concentrated solar thermochemical gasification of biomass: principles, applications, and development, Renew. Sustain. Energy Rev. 150 (2021) 111484, https://doi.org/10.1016/j.rser.2021.111484.
[11] Y. Wang, G. Li, Z. Liu, P. Cui, Z. Zhu, S. Yang, Techno-economic analysis of biomass-to-hydrogen process in comparison with coal-to-hydrogen process, Energy 185 (2019) 1063–1075, https://doi.org/10.1016/j.energy.2019.07.119.
[12] X. Li, P. Yan, C. Ma, J. Wang, Structural design and optimization of a solar spouted bed reactor of biomass gasification, Appl. Therm. Eng. 194 (2021) 117058, https://doi.org/10.1016/j.applthermaleng.2021.117058.
[13] H. Song, G. Yang, P. Xue, Y. Li, J. Zou, S. Wang, H. Yang, H. Chen, Recent development of biomass gasification for H_2 rich gas production, Applications in Energy and Combustion Science 10 (2022) 100059, https://doi.org/10.1016/j.jaecs.2022.100059.
[14] Y. Makkawi, M. Ibrahim, N. Yasir, O. Moussa, Solar-thermal conversion of biomass: principles of solar concentrators/reactors, reported studies, and prospects for large-scale implementation, Fuel Process. Technol. 264 (2024) 108139, https://doi.org/10.1016/j.fuproc.2024.108139.
[15] D. Xu, X. Gu, Y. Dai, Concentrating solar assisted biomass-to-fuel conversion through gasification: a review, Front. Energy Res. 10 (2023) 1029477, https://doi.org/10.3389/fenrg.2022.1029477.
[16] H. Wu, B. Zhang, W. Qu, R. Xu, Q. Liu, Integration of a thermochemical energy system driven by solar energy and biomass for natural gas and power production,

Sci. China Technol. Sci. 65 (2022) 1383–1395, https://doi.org/10.1007/s11431-021-2002-3.
[17] Z. Xu, S. Shan, Q. Zhang, L. Miao, Z. Zhou, Energy characteristic of concentrated solar coal gasification system based on experiment and model analysis, Sol. Energy 279 (2024) 112846, https://doi.org/10.1016/j.solener.2024.112846.
[18] C. Ma, Y. Zhou, J. Wang, X. Li, Numerical study on solar spouted bed reactor for conversion of biomass into hydrogen-rich gas by steam gasification, Int. J. Hydrogen Energy 45 (2020) 33136–33150, https://doi.org/10.1016/j.ijhydene.2020.09.120.
[19] N. Gokon, T. Izawa, T. Kodama, Steam gasification of coal cokes by internally circulating fluidized-bed reactor by concentrated Xe-light radiation for solar syngas production, Energy 79 (2015) 264–272, https://doi.org/10.1016/j.energy.2014.11.012.
[20] F. Müller, H. Patel, D. Blumenthal, P. Poživil, P. Das, C. Wieckert, P. Maiti, S. Maiti, A. Steinfeld, Co-production of syngas and potassium-based fertilizer by solar-driven thermochemical conversion of crop residues, Fuel Process. Technol. 171 (2018) 89–99, https://doi.org/10.1016/j.fuproc.2017.08.006.
[21] A. Arriagada, R. Mena, N. Ripoll, R.E. Hayes, P.A. Nikrityuk, M. Toledo, Solar-driven gasification for syngas production at low temperatures using a rotary hybrid porous media reactor, Chem. Eng. J. 495 (2024) 153011, https://doi.org/10.1016/j.cej.2024.153011.
[22] X. Zhou, J. Fu, S. Chen, CFD-DEM investigation of flow and heat transfer characteristics in a directly irradiated fluidized bed, Chem. Eng. J. 476 (2023) 146631, https://doi.org/10.1016/j.cej.2023.146631.
[23] T. Dai, C. Xu, Q. Zhang, X. Liu, Z. Chang, Y. Yang, Experimental study of the solar-driven steam gasification of coal in an improved updraft combined drop-tube and fixed-bed reactor, Energ. Conver. Manage. 259 (2022) 115571, https://doi.org/10.1016/j.enconman.2022.115571.
[24] S. Chuayboon, S. Abanades, Continuous solar-driven gasification of oil palm agricultural bio waste for high-quality syngas production, Waste Manag. 154 (2022) 303–311, https://doi.org/10.1016/j.wasman.2022.10.015.
[25] S. Wang, X. Zhu, Y. Liu, Z. Bai, Q. Liu, X. Huang, H. Wang, F. Jiao, Design and experimental study of solar-driven biomass gasification based on direct irradiation solar thermochemical reactor, Chem. Eng. J. 500 (2024) 157062, https://doi.org/10.1016/j.cej.2024.157062.
[26] Q. Zhang, S. Shan, J. Yu, Z. Zhou, K.H. Luo, Coal gasification process driven by concentrated solar radiation for carbon neutralization: reaction and energy characteristics, Chem. Eng. J. 450 (2022) 138286, https://doi.org/10.1016/j.cej.2022.138286.
[27] D. Zhong, J. Li, J. Li, X. Chen, K. Zeng, G. Flamant, H. Yang, H. Chen, Overlooked non-homogeneous effects in solar gasification of biomass, Chem. Eng. J. 504 (2025) 158751, https://doi.org/10.1016/j.cej.2024.158751.
[28] D. Zhao, T. Wu, J. Wang, S. Ling, H. Wang, H. Liu, H. Liu, S. Guo, X. Wei, Study of enhanced gasification of biochar by non-thermal concentrating solar power using novel high-flux solar simulator thermogravimetric analyzer system, Renew. Energy 242 (2025) 122436, https://doi.org/10.1016/j.renene.2025.122436.
[29] K.W. Kuttin, H. Yu, M. Yang, L. Ding, X. Chen, G. Yu, F. Wang, Experimental and numerical modeling of carbonized biomass gasification: a critical review, green Carbon 2 (2024) 176–196, https://doi.org/10.1016/j.greenca.2024.04.003.
[30] D. Yadav, R. Banerjee, A review of solar thermochemical processes, Renew. Sustain. Energy Rev. 54 (2016) 497–532, https://doi.org/10.1016/j.rser.2015.10.026.
[31] Y. Yang, R. Diao, Z. Luo, X. Zhu, Co-combustion performances of biomass pyrolysis semi-coke and rapeseed cake: PCA, 2D-COS and full range prediction of M-DAEM via machine learning, Renew. Energy 219 (2023) 119448, https://doi.org/10.1016/j.renene.2023.119448.
[32] M. Dammann, U. Santo, D. Böning, H. Knoch, M. Eberhard, T. Kolb, Entrained flow gasification: pilot-scale experimental, balancing and equilibrium data for model validation, Fuel 382 (2025) 132809, https://doi.org/10.1016/j.fuel.2024.132809.
[33] X. Yang, D. Zhong, K. Zeng, J. Li, X. Chen, H. Yang, H. Chen, Performance analysis of a novel biomass thermochemical conversion Cascade utilization system driven by concentrated solar energy, Energy (2025) 135803, https://doi.org/10.1016/j.energy.2025.135803.
[34] Ö. Tezer, N. Karabağ, A. Öngen, C.Ö. Çolpan, A. Ayol, Biomass gasification for sustainable energy production: a review, Int. J. Hydrogen Energy 47 (2022) 15419–15433, https://doi.org/10.1016/j.ijhydene.2022.02.158.
[35] Y. Yao, A. Panahi, Y.A. Levendis, Comparative radiative property measurements of single biomass and coal particles burning at high reactor temperatures, Combust. Flame 263 (2024) 113406, https://doi.org/10.1016/j.combustflame.2024.113406.
[36] M. Koch, S. Pielsticker, R. Kneer, Biomass particle-radiation-interaction and the effect of shape and structure simplifications, Fuel 361 (2024) 130657, https://doi.org/10.1016/j.fuel.2023.130657.
[37] J. Yu, S. Shan, Q. Zhang, X. Wang, G. Jin, Z. Zhou, Thermal radiation characteristic parameters of biomass mixed feedstock for concentrating solar gasification reaction, Thermal Science and Engineering Progress 54 (2024) 102791, https://doi.org/10.1016/j.tsep.2024.102791.
[38] B. Xie, W. Zhang, J. Zhao, C. Zheng, L. Liu, Design of VO_2-based spacecraft smart radiator with low solar absorptance, Appl. Therm. Eng. 236 (2024) 121751, https://doi.org/10.1016/j.applthermaleng.2023.121751.
[39] S. Chuayboon, S. Abanades, S. Rodat, Experimental analysis of continuous steam gasification of wood biomass for syngas production in a high-temperature particle-fed solar reactor, Chemical Engineering and Processing - Process Intensification 125 (2018) 253–265, https://doi.org/10.1016/j.cep.2018.02.004.
[40] B. Rahmatmand, S.K. Rish, A. Jayasekara, H. Lomas, P. Koshy, L. North, A. Tahmasebi, Gasification and degradation mechanism of metallurgical coke in CO_2 and H_2O using the random pore model with intraparticle diffusion, Fuel 383 (2025) 133859, https://doi.org/10.1016/j.fuel.2024.133859.
[41] G. Wang, J. Zhang, J. Shao, Z. Liu, H. Wang, X. Li, P. Zhang, W. Geng, G. Zhang, Experimental and modeling studies on CO_2 gasification of biomass chars, Energy 114 (2016) 143–154, https://doi.org/10.1016/j.energy.2016.08.002.
[42] H. Boujjat, S. Rodat, S. Chuayboon, S. Abanades, Experimental and numerical study of a directly irradiated hybrid solar/combustion spouted bed reactor for continuous steam gasification of biomass, Energy 189 (2019) 116118, https://doi.org/10.1016/j.energy.2019.116118.
[43] A.I. Ferreiro, A.F. Ferreira, E.C. Fernandes, P. Coelho, Influence of process parameters on biomass gasification: a review of experimental studies in entrained flow reactors and droptube furnaces, Biomass Bioenergy 185 (2024) 107217, https://doi.org/10.1016/j.biombioe.2024.107217.
[44] Y. Liu, D. Bi, M. Yin, K. Zhang, H. Liu, S. Liu, Modeling and exergy-economy analysis of residential building energy supply systems combining torrefied biomass gasification and solar energy, Thermal Science and Engineering Progress 50 (2024) 102584, https://doi.org/10.1016/j.tsep.2024.102584.
[45] K. Mielke, T. Kolb, M. Müller, Chemical fractionation of inorganic constituents in entrained flow gasification of slurry from straw pyrolysis, Biomass Bioenergy 141 (2020) 105732, https://doi.org/10.1016/j.biombioe.2020.105732.
[46] C.B. Felix, W.H. Chen, A.T. Ubando, Y.K. Park, K.Y.A. Lin, A. Pugazhendhi, T. B. Nguyen, C. Dong, A comprehensive review of thermogravimetric analysis in lignocellulosic and algal biomass gasification, Chem. Eng. J. 445 (2022) 136730, https://doi.org/10.1016/j.cej.2022.136730.
[47] J. Zhang, J. Li, Y. Mao, J. Bi, M. Zhu, Z. Zhang, L. Zhang, D. Zhang, Effect of $CaCO_3$ addition on ash sintering behaviour during K_2CO_3 catalysed steam gasification of a Chinese lignite, Appl. Therm. Eng. 111 (2017) 503–509, https://doi.org/10.1016/j.applthermaleng.2016.09.111.
[48] Y. Wu, H. Wang, H. Li, X. Han, M. Zhang, Y. Sun, X. Fan, R. Tu, Y. Zeng, C.C. Xu, X. Xu, Applications of catalysts in thermochemical conversion of biomass (pyrolysis, hydrothermal liquefaction and gasification): a critical review, Renew. Energy 196 (2022) 462–481, https://doi.org/10.1016/j.renene.2022.07.031.
[49] R.D. Gómez-Vásquez, E.A. Castiblanco, Z. Zapata Benabithe, A.J. Bula Silvera, D. A. Camargo-Trillos, Photochromic single atom Ag/TiO_2 catalysts for selective CO_2 reduction to CH_4, Biomass Bioenergy 153 (2021) 106207, https://doi.org/10.1016/j.biombioe.2021.106207.
[50] L. Wei, Z. Pan, S. Sun, Z. Yi, G. Li, L. An, A novel electro-assisted thermochemical reactor for conversion of CO_2/H_2O into solar fuels, Int. J. Heat Mass Transf. 229 (2024) 125742, https://doi.org/10.1016/j.ijheatmasstransfer.2024.125742.